(12) INTERNATIONAL APPLICATION PUBLISHED UNDER THE PATENT COOPERATION TREATY (PCT)

(19) World Intellectual Property Organization
International Bureau

(43) International Publication Date
22 November 2012 (22.11.2012)

WIPO | PCT

(10) International Publication Number
WO 2012/156332 A1

(51) International Patent Classification:
C01B 3/00 (2006.01) *C01B 3/02* (2006.01)

(21) International Application Number:
PCT/EP2012/058832

(22) International Filing Date:
11 May 2012 (11.05.2012)

(25) Filing Language: English

(26) Publication Language: English

(30) Priority Data:
PCT/EP2011/058164 19 May 2011 (19.05.2011) EP
PCT/EP2011/060823 28 June 2011 (28.06.2011) EP

(71) Applicant *(for all designated States except US)*: **UNIVERSITÉ CATHOLIQUE DE LOUVAIN** [BE/BE]; Place de l'Université 1, Louvain-la-Neuve, B-1348 Louvain-la-Neuve (BE).

(72) Inventors; and
(75) Inventors/Applicants *(for US only)*: **PROOST, Joris** [BE/BE]; Tiensesteenweg 315, B-3010 Kessel-Lo (BE). **DELMELLE, Renaud** [BE/BE]; Rue des Faucons 59, B-5004 Bouge (BE). **MICHOTTE, Sébastien** [BE/BE]; Venelle du Bois Saras 30, B-1300 Wavre (BE).

(74) Agent: **BRANTS, Johan, Philippe, Emile**; Brantsandpatents bvba, Guldensporenpark 75, B-9820 Merelbeke (BE).

(81) Designated States *(unless otherwise indicated, for every kind of national protection available)*: AE, AG, AL, AM, AO, AT, AU, AZ, BA, BB, BG, BH, BR, BW, BY, BZ, CA, CH, CL, CN, CO, CR, CU, CZ, DE, DK, DM, DO, DZ, EC, EE, EG, ES, FI, GB, GD, GE, GH, GM, GT, HN, HR, HU, ID, IL, IN, IS, JP, KE, KG, KM, KN, KP, KR, KZ, LA, LC, LK, LR, LS, LT, LU, LY, MA, MD, ME, MG, MK, MN, MW, MX, MY, MZ, NA, NG, NI, NO, NZ, OM, PE, PG, PH, PL, PT, QA, RO, RS, RU, RW, SC, SD, SE, SG, SK, SL, SM, ST, SV, SY, TH, TJ, TM, TN, TR, TT, TZ, UA, UG, US, UZ, VC, VN, ZA, ZM, ZW.

(84) Designated States *(unless otherwise indicated, for every kind of regional protection available)*: ARIPO (BW, GH, GM, KE, LR, LS, MW, MZ, NA, RW, SD, SL, SZ, TZ, UG, ZM, ZW), Eurasian (AM, AZ, BY, KG, KZ, RU, TJ, TM), European (AL, AT, BE, BG, CH, CY, CZ, DE, DK, EE, ES, FI, FR, GB, GR, HR, HU, IE, IS, IT, LT, LU, LV, MC, MK, MT, NL, NO, PL, PT, RO, RS, SE, SI, SK, SM, TR), OAPI (BF, BJ, CF, CG, CI, CM, GA, GN, GQ, GW, ML, MR, NE, SN, TD, TG).

Declarations under Rule 4.17:

— *of inventorship (Rule 4.17(iv))*

Published:

— *with international search report (Art. 21(3))*

WO 2012/156332 A1

(54) **Title**: DEVICE, METHOD AND SYSTEM FOR IMPROVED UPTAKE, STORAGE AND RELEASE OF HYDROGEN

(57) **Abstract**: The current invention concerns a device for the improved uptake, storage and release of hydrogen, comprising a solid-state active element capable of taking up, storing and releasing hydrogen; and stress-inducing means attached to the active element, characterized in that said stress-inducing means are capable of applying a mechanical load to the active element. Furthermore, the current invention also concerns a system and methods for the improved uptake, storage and release of hydrogen.

DEVICE, METHOD AND SYSTEM FOR IMPROVED UPTAKE, STORAGE AND RELEASE OF HYDROGEN

TECHNICAL FIELD

The invention pertains to the technical field of hydrogen storage, more in particular the invention provides devices, methods and systems for the improved uptake, storage and release of hydrogen for hydrogen fuel cell applications.

BACKGROUND

It is generally recognised that, with an ever increasing energy demand for mobility and transport applications, hydrogen appears to be a good fuel candidate to replace conventional hydrocarbons. The intrinsic obstacle to industrial applications is the hydrogen volatility, which makes hydrogen storage technologically challenging. Many potential solutions already exist, but most of them suffer from a lack of economic competitiveness as compared to current fuels. Metallic hydrides bring a totally different perspective to this debate. They may allow a solid-state hydrogen storage application.

With the perspective of hydrogen being used as the major future energy carrier for transport applications, its storage is a critical technological issue. Consensus still needs to be reached by industry on the exact chemical composition of the most suitable material for solid-state hydrogen storage. However, the current invention provides a novel and inventive way to increase both the hydrogen storage capacity, as well as the rate of hydrogen uptake and release for any given solid material, by applying a mechanical stress. The effect of the mechanical stress is to alter the crystal structure of material of which a solid-state hydrogen storage device is made, in such a way that the physical and chemical properties of the material are more apt to take up, release or store hydrogen. More in particular, by controlling the mechanical stress, the adsorption of H_2 at the surface, the dissociation of H_2 into 2H, the migration and absorption of hydrogen into the bulk of a thin-film layer, and the equilibrium concentration of H or H-storing capacity in the layer can be improved, thereby increasing the uptake and storage of hydrogen in a thin film; by changing the mechanical stress, the equilibrium concentration of H or H-storing capacity in the layer can be changed, the migration of hydrogen from the bulk of the

thin film to the surface can be increased, the forming of H_2 from 2H at the surface and the desorption of H_2 can be improved, thereby increasing the rate of hydrogen release.

The current major bottleneck in solid state hydrogen storage technology, which is the technology envisioned for future electrical vehicles, is the intrinsic compromise between the ease of hydrogen uptake and the ability for a quick hydrogen release. Both requirements are indeed difficult to combine, since a material with a high chemical affinity for hydrogen, i.e. a material which easily takes up hydrogen, will most likely have great difficulty to release it. This is due to the processes governing the hydrogen uptake, storage and release, which are typically equilibrium reactions determined by thermodynamic properties on the one hand and by the activation energies which are characteristic for the processes involved on the other hand. These activation energies are determined by the composition and structure of the material, and in previous applications, the reactions were steered by controlling the thermodynamic properties of the environment, such as temperature, pressure and H_2 partial pressure, while the activation energies remained constant. In these applications, e.g. a high uptake rate can be achieved at low temperature, while a reasonable high release rate can only be achieved at increased temperature, or vice versa. For instance, Mg and its alloys, being one the major candidates for solid state hydrogen storage, currently needs to be heated up by more than 200°C before it is able to release its stored hydrogen. This temperature increase is technologically not realistic for electrical vehicles.

Baldi et al. (Phys. Rev. Lett. 102, 226102 (2009)) tuned the thermodynamics of hydrogen absorption in Mg by means of elastic clamping. The loading isotherms measured by hydrogenography show that Mg films covered with Mg-alloy-forming elements, such as Pd and Ni, have hydrogen plateau pressures more than 2 orders of magnitude higher than bulk Mg at the same temperature (see fig. 15). An elastic model allows to interpret the Mg thickness dependence of the hydrogen plateau pressure. Their results suggest an alternative route for the development of new hydrogen storage materials with optimized thermodynamic properties. However, Baldi et al. do not disclose how the uptake and release rate can be improved.

The present invention provides a different approach in order to get both large uptake and large release rates, and at the same time increase the storage capacity of the active elements of a hydrogen fuel cell. In the present invention, the

structure of the active element can be altered by stress-inducing means. By altering the stress, the lattice of the solid-state active element can be deformed, thereby altering the electronic state of both the surface and the bulk, which determines the activation energies for the different reactions involved, such as H_2-adsorption/desorption at the surface, dissociation at the surface, H-migration or diffusion from the surface to the bulk and vice versa. Thus by controlling the stress induced in the active element, one can control the activation energies, and one is thus able to increase the uptake rate, the storage capacity or the release rate of hydrogen when desired. More in particular, when an active element is depleted of hydrogen, one may reload such an element by altering the induced stress to increase the hydrogen uptake rate whilst exposing the element to a H_2-rich environment. When in a later phase hydrogen is needed for producing energy, the stress applied to a hydrogen-loaded active element can be altered in order to increase the hydrogen release rate of this active element.

The stress can be induced by applying the appropriate mechanical load, like a biaxial tension or compression, during either the hydrogen uptake or the release phase. Then, it would become possible to accelerate either the uptake or release phase without having to apply a temperature increase. Fundamentally, our tests and calculations demonstrate that this is related to a so-called mechano-chemical coupling effect, i.e. a mechanical modulation of the activation energy characteristic for hydrogen uptake or release. Such a modulation has, to the best of our knowledge, never been tested before for hydrogen storage applications. A potential implementation could in our opinion consist of adapting existing hydrogen storage devices so that they can support the appropriate mechanical load, preferably biaxial tension and/or compression.

In a first aspect, the present invention thus provides a device or active element for the improved uptake, release and storage of hydrogen.

In a second aspect, the present invention provides a system for the improved uptake, release and storage of hydrogen.

In a third aspect, the present invention provides methods for the improved uptake, release and storage of hydrogen.

SUMMARY OF THE INVENTION

The present invention provides a device for the improved uptake, storage and release of hydrogen, comprising:
- a solid-state active element capable of taking up, storing and releasing hydrogen; and
- stress-inducing means attached to the active element,

characterized in that said stress-inducing means are capable of applying a mechanical load to the active element.

By controlling the internal stress in the active element by the stress-inducing means, one can:
- improve the hydrogen uptake rate of the active element;
- improve the hydrogen storage capability of the active element; and/or
- improve the hydrogen release rate of the active element,

due to the mechano-chemical coupling effect described above. Furthermore, the use of a solid-state active element increases security, stability and easiness of manufacturing.

The mechanical load that can be induced by the stress-inducing means can be any kind of load which is beneficial for the improved uptake, storage and/or release of hydrogen by the active element. In a preferred embodiment, the load leads to uniaxial tension or compression, biaxial tension or compression, triaxial tension or compression, bending, torsion, or any combination thereof.

In an embodiment, the present invention provides a device such as described before, whereby said stress-inducing means comprise an electromechanical device attached to at least one side of the active element, said electromechanical device capable of pushing and pulling at said side of said active element thereby capable of inducing compressive or tensile stress in the active element, said electromechanical device controlled by an electrical control circuit.

In another embodiment, the present invention provides a device such as described before, whereby said solid-state active element comprises a thin-film on a substrate.

In a preferred embodiment, the thin film may be a metallic thin film or it may comprise metals or an alloy. In a more preferred embodiment, the thin film may comprise Mg, Pd, transition metal hydrides, borohydrides, amidoboranes and combinations or alloys thereof.

In a preferred embodiment, the substrate of an active element may comprise a metal, an alloy, a polymer, a ceramic, a monocrystalline solid, Si, KBr or any combination thereof.

In an embodiment, the present invention provides a device such as described before, whereby said active element is mounted on a fixed frame at or near the in-plane sides of said active element and said stress-inducing means comprise at least one piezo-electric crystal located at or near the middle of said active element and capable of pushing or pulling at said substrate and said thin film of said active element, thereby capable of bending said active element out of its plane.

If the active element comprises a thin film on a substrate, the thin film identifies a two-dimensional surface which is flat or has a very small curvature, i.e. the radius of curvature is much larger than the width or length of the thin film-surface. With "in-plane sides" are meant the sides of the active element which are basically in the plane of the thin film surface. For example, if the active element has the form of a cylinder with large radius and small height, the in-plane side is the side-surface of the cylinder and not the top or bottom.

When the active element is thusly attached to a frame, it suffices to apply a mechanical load at one or more places near the middle of the surface in order to induce a stress everywhere in the thin film. One way of doing this is by placing a piezo-electric crystal at or near the middle of the thin film, which one can electrically control to push or pull the substrate and thin film, thereby bending the active element. The bending induces mechanical stress in the thin film and thereby alters the hydrogen uptake, storage and release capabilities of the thin film as desired.

In an embodiment, the present invention provides a device such as described before, whereby said stress-inducing means comprise a lattice mismatch between said thin film and said substrate of said active element.

Internal stress in the thin film can be induced by a lattice mismatch, microstructurally, thermally, etc. or a combination thereof. This stress can be tensile or compressive stress or a combination, e.g. whereby the film is compressed along one axis and stretched along another. In a preferred embodiment, the lattice mismatch, microstructures, thermal conditions, etc. are chosen such that the induced internal stress is optimized for hydrogen storage, i.e. when no external stress-inducing means are present or applied, the hydrogen storage capacity of the thin film is maximized. This has the advantage of not having to apply a mechanical load by an external stress-inducing means when the active element is not being loaded or depleted, i.e. when it is not being used or recharged. Furthermore, this has the extra advantage of being more secure in that when the external stress-inducing means should fail during operation, the hydrogen is kept stored in the active element and is not released uncontrollably.

The internal stress caused by e.g. lattice mismatch, can be controlled by careful preparation of the film. When sputtering is used, the internal stress may be controlled by e.g. the Argon pressure during sputtering. Figure 19 illustrates that a different Argon pressure results in a different internal stress, even for equal thickness and grain size of thin films. This is because of the formation of columnar grains. The properties of differently prepared thin film samples such as internal stress, Pd thickness, density, grain size and texture factor, are summarized in fig. 20. It is clear that while film thickness, density, grain size and texture factor are similar for the different film samples, the internal stress displays a large dependence on the Argon pressure during sputtering.

In a second aspect, the present invention provides a system for the improved uptake, storage and release of hydrogen, comprising:
- one or more devices as described above; and
- an air-tight container in which said devices are mounted,

characterized in that said air-tight container comprises one or more in- and/or outlets for H_2-gas and one or more control mechanisms for the stress-inducing means of said one or more devices.

In a preferred embodiment the outlets of such a system are connected to a hydrogen fuel cell and are capable of feeding the fuel well with hydrogen at a predetermined temperature, pressure, partial pressure and flow rate. In another preferred embodiment, the stress-inducing means of the devices of the system are

controlled by the control mechanisms such that the uptake, storage and release of the hydrogen gas is improved for the whole system. In another embodiment, the control mechanisms comprise an electrical control circuit and/or wiring.

In a further aspect, the present invention provides a method for the improved uptake of hydrogen in a device as described above, comprising the steps of:
- applying a mechanical load to said active element of said device by said stress-inducing means; and
- bringing the surface of said active element into contact with H_2-gas under a predetermined temperature and pressure.

Such a method can be used to charge or recharge a hydrogen depleted or partially depleted active element. In a preferred embodiment, the stress induced by the stress-inducing means is optimized to allow for a maximal hydrogen uptake rate. In another preferred embodiment, the hydrogen pressure, partial pressure and/or temperature are optimized for the hydrogen uptake, i.e. the hydrogen uptake rate is maximized by controlling the thermodynamic properties during the charging of the active element.

In still a further aspect, the present invention provides a method for the improved storage of hydrogen in a device as described above, comprising the steps of:
- applying a mechanical load to said active element of said device by said stress-inducing means;

In a preferred embodiment, the stress induced by the stress-inducing means is optimized to allow for a maximal hydrogen storage capacity.

In yet a further aspect, the present invention provides a method for the improved release of hydrogen in a device as described above, comprising the steps of:
- applying a mechanical load to said active element of said device by said stress-inducing means; and
- evacuating the H_2-gas which is released by said active element.

Such a method can be used to discharge a hydrogen charged or partially charged active element. In a preferred embodiment, the stress induced by the stress-inducing means is optimized to allow for a maximal hydrogen release rate. In

another preferred embodiment, the ambient pressure, H_2-partial pressure and/or temperature are optimized for the hydrogen release, i.e. the hydrogen release rate is maximized by controlling the thermodynamic properties during the discharging of the active element.

In yet a further aspect, the present invention provides a method for providing a fuel cell with hydrogen gas, comprising the steps of:

- loading the active elements of a system as described above, by means of a charging method as described above, whereby the H_2-gas is provided via said in- or outlets of said system;
- storing hydrogen in the active elements of said system by means of a method as described above; and
- releasing hydrogen from the active elements by means of a method as described above whereby the released H_2-gas is evacuated via said in- or outlets of said system and provided to said fuel cell.

DESCRIPTION OF FIGURES

Figure 1a shows a schematic representation of the principal kinetic steps involved in Pd hydriding.

Figure 1b shows a schematic representation of the principal kinetic steps involved in Pd hydriding with an extra de-hydriding step compared to fig. 1a.

Figure 2a shows the evolution of the absolute internal stress as a function of time during a hydriding cycle recorded at p_{H2} = 6 mbar. Inset: hydriding cycle recorded at p_{H2} = 5.5 mbar, including venting with air after dehydriding in vacuum.

Figure 2b shows the inset of fig. 2a separately.

Figure 3 shows the equilibrium absolute stress as a function of p_{H2}. The average initial tensile growth stress in the as-deposited films was 409 ± 2 MPa.

Figure 4 shows the equilibrium absolute stress as a function of $(p_{H2})^{1/2}$ in the α phase region.

Figure 5a shows the slope of the first linear kinetic regime as a function of $1/(p_{H2})^{1/2}$.

Figure 5b shows the slope of the first linear kinetic regime as a function of $1/(p_{H2})^{1/2}$ for samples under different mechanical stress.

Figure 6a shows the slope of the second linear kinetic regime as a function of p_{H2}.

Figure 6b shows the slope of the second linear kinetic regime as a function of p_{H2} for samples under different mechanical stress.

Figure 7 shows the transition time between the first and second kinetic regime as a function of p_{H2}. A schematic construction indicating the definition of t_{tr} and I_σ in Eq. (24) is included as well.

Figure 8 shows the evolution of the bulk atomic concentration n in the third, non-linear kinetic regime for different values of p_{H2}. The time scale has been shifted so that t = 0 sec corresponds to the transition between the second and third kinetic regime. The coarse solid lines correspond to a fit using Eq. (30).

Figure 9 shows a schematic representation of the θ-dependencies of the adsorption (r_{ad}) and absorption (r_{ab}) velocities, superimposed on the experimentally measured hydriding cycle at p_{H2} = 6 mbar. Fits to the experimental data have been included as well, using constitutive eq. (30) for the absorption-controlled first and third regime, and eq. (19) for the second, adsorption-limited regime. The values mentioned for k'_{ab} in regime I and III represent average values derived from the fitting parameter C_2 (cfr. eq. (29)) when including all experiments.

Figure 10a shows the measured curvature change of a Pd thin film during a first period of a hydriding cycle, whereby two samples have been measured: one sample had an internal stress of 100 MPa, the other had an internal stress of 358 MPa; these stresses were induced due to lattice mismatches between thin film and substrate.

Figure 10b shows similar curves as fig. 10a, but for three samples under different internal tensile and compressive stresses 272 MPa, 61 MPa and -55 MPa.

Figure 11 shows the kinetics involved in a hydriding cycle of a Pd thin film as known from previous work.

Figure 12 shows the compressive stress change of a Pd thin film and of a substrate without Pd film during a first period of a hydriding cycle.

Figure 13 shows the kinetics involved in a hydriding cycle of a Pd thin film when being submitted to tensile stress.

Figure 14 shows the measured hydrogen uptake of a Pd thin film during a first period of a hydriding cycle, whereby two samples have been measured: one sample had an internal stress of 100 MPa, the other had an internal stress of 358 MPa; these stresses were induced due to lattice mismatches between thin film and substrate.

Figure 15 shows loading isotherms measured by hydrogenography in which Mg films covered with Mg-alloy-forming elements, such as Pd and Ni, have hydrogen plateau pressures more than 2 orders of magnitude higher than bulk Mg at the same temperature.

Figure 16 shows the Pd-H phase diagram.

Figure 17 shows the curvature measurement setup and the reflected laser spots in the CCD which change with the curvature of the sample.

Figure 18 shows the change in internal stress in a Pd layer, which is a result of the prohibited volume change during Pd-H interaction in the thin film geometry with a Pd film on a substrate.

Figure 19 shows that a different Argon pressure results in a different internal stress, even for equal thickness and grain size of thin films.

Figure 20 summarizes the properties of differently prepared thin film samples such as internal stress, Pd thickness, density, grain size and texture factor.

Figure 21 shows the evolution of the heat of adsorption and the decrease of the heat of adsorption caused by the mechanical stress on the film.

Figure 22 shows the linear evolution of the absorption rate constant $k'_{ab,I}$ in the first kinetic regime with the hydrogen partial pressure and its dependence on the mechanical stress.

Figure 23 shows how applying mechanical stress may improve the activation volume for hydrogen absorption.

Figure 24 shows the dependence of Sievert's constant on the internal stress.

Figure 25 illustrates the evolution of the stress*thickness product as a function of time (before and during Ti layer deposition, as well as after Pd deposition) and Pd thickness (during Pd deposition) using different argon sputtering pressures.

Figure 26 illustrates the evolution of the compressive stress change as a function of time during three hydriding cycles recorded using samples exhibiting different growth-induced stresses.

Figure 27 illustrates the room temperature pressure-absolute stress isotherms of the 5 sets of samples presented in Table 2, obtained by successively introducing small amounts of hydrogen into the chamber and waiting for equilibrium.

Figure 28 illustrates the slope of the first linear kinetic regime as a function of p_{H2}, fitted with Eq. (18) and including the p_{H2}-dependence of k'_{ab} (Eq. (32)).

Figure 29 illustrates the slope of the second linear kinetic regime as a function of p_{H2}, fitted with Eq. (19) with one single fit for the three sets of samples.

Figure 30 illustrates the rate constant for hydrogen absorption as a function of p_{H2}. Linear fits are shown for each set of samples.

Figure 31 illustrates a schematic energy level diagram for H adsorption/absorption into palladium, showing the effect of internal stress on the activation enthalpy for hydrogen absorption.

Figure 32 illustrates the slopes of the linear fits of Fig. 30 as a function of σ_0.

Figure 33 illustrates the evolution of the bulk atomic hydrogen concentration n in the third, non-linear kinetic regime for different values of p_{H2} (σ_0 = 61 MPa). The time scale is normalised to represent for each experiment the first 40s of the third kinetic regime. The coarse solid lines correspond to a fit using Eq. (30).

DETAILED DESCRIPTION OF THE INVENTION

The present invention concerns a device, a system and a method for the improved uptake, storage and release of hydrogen, which can be used in hydrogen fuel cells for the production of energy.

Unless otherwise defined, all terms used in disclosing the invention, including technical and scientific terms, have the meaning as commonly understood by one of ordinary skill in the art to which this invention belongs. By means of further guidance, term definitions are included to better appreciate the teaching of the present invention.

As used herein, the following terms have the following meanings:

"A", "an", and "the" as used herein refers to both singular and plural referents unless the context clearly dictates otherwise. By way of example, "a compartment" refers to one or more than one compartment.

"About" as used herein referring to a measurable value such as a parameter, an amount, a temporal duration, and the like, is meant to encompass variations of +/-20% or less, preferably +/-10% or less, more preferably +/-5% or less, even more preferably +/-1% or less, and still more preferably +/-0.1% or less of and from the specified value, in so far such variations are appropriate to perform in the disclosed invention. However, it is to be understood that the value to which the modifier "about" refers is itself also specifically disclosed.

"Comprise," "comprising," and "comprises" and "comprised of" as used herein are synonymous with "include", "including", "includes" or "contain", "containing", "contains" and are inclusive or open-ended terms that specifies the presence of what follows e.g. component and do not exclude or preclude the presence of

additional, non-recited components, features, element, members, steps, known in the art or disclosed therein.

The recitation of numerical ranges by endpoints includes all numbers and fractions subsumed within that range, as well as the recited endpoints.

The expression "% by weight" (weight percent), here and throughout the description unless otherwise defined, refers to the relative weight of the respective component based on the overall weight of the formulation.

The expression "stress" refers to all kinds of mechanical stresses in a material, independently of whether it is normal or shear stress, tensile or compressive stress, or any combination thereof. Furthermore, the stress can relate to stress in all possible directions and can be direction dependent. In general, the stress in a material can be parameterized by a symmetric 3 by 3 stress tensor, of which the elements can be real-valued functions depending on position.

The expression "active element" refers to a part of the device or system in which the hydrogen can be taken up, stored for a certain period and released.

With the perspective of hydrogen being used as the major future energy carrier for transport applications, especially electric cars, its storage is still a critical technological issue. While consensus still needs to be reached by industry on the exact chemical composition of the most suitable material for solid state hydrogen storage, the current invention provides a novel way to increase both the hydrogen storage capacity, as well as the rate of hydrogen uptake and release for any given solid material, by applying a mechanical stress. In this respect, our tests have demonstrated that for a model nano-crystalline metallic thin film system, a 30% increase in the rate of hydrogen uptake, and a 3% increase in storage capacity at ambient temperature for a given hydrogen partial pressure can be achieved. These numbers are significant, as they are of the same order of magnitude as currently reported improvements by optimising the chemical composition.

Moreover, by applying the appropriate mechanical load during either the hydrogen uptake or the release phase, it would become possible to accelerate either the uptake or release phase without having to apply a temperature increase. Fundamentally, our tests and calculations demonstrate that this is related to a so-called mechano-chemical coupling effect, i.e. a mechanical modulation of the

activation energy characteristic for hydrogen uptake or release. Such a modulation has, to the best of our knowledge, never been tested before for hydrogen storage applications.

The effect is universally applicable to any solid material, as long as the applied load stays in the elastic regime. The potential benefit can therefore also be expected to scale with the ability of the candidate storage material to deform elastically. A potential implementation could in our opinion consist of adapting existing hydrogen storage devices so that they can support the appropriate mechanical load.

In a first aspect, the invention provides a device for the improved uptake, storage and release of hydrogen. Such device comprises an active element and stress-inducing means.

The stress-inducing means may comprise a mechanical load, a magnetic installation, an electric installation, an electromagnetic installation, a piezo-electric installation, etc.

In a preferred embodiment, the active element is fixed near its sides to a solid frame and can be bent by at least one mechanical, magnetic, electric, electromagnetic, piezo-electric, hydraulic, pneumatic or other type of device which is capable of pushing or pulling the active element at or near the middle.

In another preferred embodiment, the chemical composition of the active element is optimized for the uptake, storage and release of hydrogen.

In an embodiment, the active element comprises a thin film, which may be a metallic film, which may comprise Pd or Mg and the active element may comprise a substrate which may comprise a polymer, a ceramic or a monocrystalline material and may comprise Si and/or KBr.

Internal stresses in the active element may be due to film-substrate lattice mismatch, mechanically, magnetically, electrically, electromagnetically, microstructurally, thermally induced stresses. The induced stresses may be biaxial tensile/compression stress, bending stresses, torsion stress, tensile and/or compressive uniaxial or tri-axial stresses, etc.

The use of thin film model systems generally allows to separate more easily the different rate-controlling kinetic steps involved during hydriding. A recent study by S. Wagner and A. Pundt, (Applied Physics Letters 92, 051914/1-3 (2008)) has suggested that some of the thermodynamic parameters governing such thin film hydriding cycles are influenced by mechanical stress in the as-deposited film. In order to come to the present invention, we have first measured this effect in quantitative detail, using a high resolution curvature measurement setup (R. Delmelle, G. Bamba, J. Proost, International Journal of Hydrogen Energy 35 (2010), p. 9888-9892). In the thin film geometry, such curvature changes during hydriding arise from the constrained volume expansion upon interaction of hydrogen with the thin film. In the case of room temperature Pd hydriding, shown as an example in Figs. 10a and 10b, the first kinetic regime observed directly after H_2 introduction in a high vacuum chamber is significantly enhanced by the presence of tensile internal stress, while the second one essentially remains unaffected. Figures 10a and 10b in this example also show that tensile stresses may accelerate kinetics while compressive stresses may slow down the kinetics. In previous work (Renaud Delmelle and Joris Proost, Physical Chemistry Chemical Physics (2011) DOI: 10.1039/c0cp02773a), we have presented a quantitative kinetic of full hydriding cycles, allowing to extract relevant kinetic and thermodynamic hydriding parameters, like the equilibrium H-concentration, the α to β phase transition pressure and the hydrogen ad- and absorption velocities, based on a self-consistent kinetic model able to describe the complete room temperature Pd hydriding cycle.

Study A: In-situ study of the hydriding kinetics of Pd thin films

An in situ study of the hydriding kinetics of Pd thin films was performed recently. In the following, reference is made to the following publications:

[1] E. Wicke and H. Brodowsky, In: G. Alefeld and J.Voelkl (Eds.) *Hydrogen in metals vol. 2*, pp. 73-155, Springer, Berlin, Germany, 1978.

[2] F. A. Lewis, *The palladium hydrogen system*, Academic Press, London, UK, 1967.

[3] E. L. Fleischer (Ed.), *MRS Bulletin*, Volume 27, No. 9, pp. 675-716, Franklin Design and SPI Technologies, Warrendale, USA, 2002.

[4] P. Chen and M. Zhu, *Materials Today* 11 (2008) 36-43.

[5] R. -H. Jones and G. Thomas, *JOM* 59 (2007) 50-55.

[6] Z. Zhao, Y. Sevryugina, M. A. Carpenter, D. Welch and H. Xia, *Anal. Chem.* 76 (2004) 6321-6326.

[7] A. Kulprathipanja, G. O. Alptekin, J. L. Falconer and J. D. Way, *J. Membrane Sci.* 254 (2005) 49-62.

[8] L. L. Jewell and B. H. Davis, *Applied catalysis A: General* 310 (2006) 1-15.

[9] Z. Hu, T. Thundat and R.J. Warmack, *J. Appl. Phys.* 90 (2001) 427-431.

[10] W. Vogel, W. He, Q. -H. Huang, Z. Zou, X. -G. Zhang and H. Yang, *Int. J. Hydrogen Energy* 35 (2010) 8609-8620.

[11] M. Suleiman, N. M. Jisrawi, O. Dankert, M. T. Reetz, C. Bähtz, R. Kircheim and A. Pundt, *J. Alloys Comp.* 356-357 (2003) 644-648.

[12] A. Pundt and R. Kircheim, *Annu. Rev. Mater. Res.* 36 (2006) 555-608.

[13] R. J. Matelon, J. I. Avila, U. G. Volkmann, A. L. Cabrera, E. H. Morales and D. Lederman, *Thin Solid Films* 516 (2008) 7797-7801.

[14] T.P. Leervad Pedersen, C. Liesch, C. Salinga, T. Eleftheriadis, H. Weis and M. Wuttig, *Thin Solid Films* 458 (2004) 299-303.

[15] C. Lemier and J. Weissmüller, *Acta Mater.* 55 (2007) 1241-1254.

[16] M. Pasturel, M. Slaman, H. Schreuders, J. H. Rector, D. M. Borsa, B. Dam and R. Griessen, *J. Appl. Phys.* 100 (2006) 023515/1-8.

[17] R. Delmelle, G. Bamba and J. Proost, *Int. J. Hydrogen Energy* 35 (2010) 9888-9892.

[18] Q. Van Overmeere, J.-F. Vanhumbeeck and J. Proost, *Rev. Sci. Instrum.* 81 (2010) 045106/1-10.

[19] J. Proost and F. Spaepen, *J. Appl. Phys.* 91 (2002) 204-216.

[20] N. Joshi, D. K. Aswal, A. K. Debnath, S. K. Gupta and J. V. Yakhmi, *Appl. Surf. Sci.* 228 (2004) 302-305.

[21] U. Singh, N. Jha, T. P. Singh, A. Kapoor and A. Perrone, *Opt. Laser Technol.* 42 (2010) 1128-1133.

[22] S. Bouhtiyya and L. Roué, *Int. J. Hydrogen Energy* 33 (2008) 2912-2920.

[23] A. Kern and W. Eysel, Mineralogisch-Petrograph. Inst., Univ. Heidelberg, Germany, ICDD Grant-in-Aid, 1993.

[24] M. M. El Gowini and W. A. Moussa, *Sensors* 10 (2010) 1232-1250.

[25] H. Peisl, In: G. Alefeld and J.Voelkl (Eds.) *Hydrogen in metals vol. 1*, pp. 57-73, Springer, Berlin, Germany, 1978.

[26] A. Pundt, E. Nikitin, P. Pekarski and R. Kirchheim, *Acta Mater.* 52 (2004) 1579-1587.

[27] P. G. Sanders, J. A. Eastman and J. R. Weertman, *Acta Mater.* 45 (1997) 4019-4025.

[28] C. J. Smithells, *Metals reference book*, p. 1258, Butterworths, London, UK, 2004.

[29] R. V. Bucur, *J. Mat. Sci.* 22 (1987) 3402-3406.

[30] R.V. Bucur, *Surface Science* 62 (1977) 519-535.

[31] M. Johansson, E. Skúlason, G. Nielsen, S. Murphy, R. M. Nielsen and I. Chorkendorff, *Surface Science* 604 (2010) 718-729.

[32] S. Hong and T. S. Rahman, *Phys. Rev. B* 75 (2007) 155405/1-10.

[33] T. L. Ward and T. Dao, *J. Membrane Sci.* 153 (1999) 211-231.

[34] J. B. Rawlings and J. G. Ekerdt, *Chemical reactor analysis and design fundamentals*, pp.189-277, Nob Hill Pub., Madison, USA, 2002.

[35] G. G. Froment, K. B. Bischoff and J. De Wilde, *Chemical reactor analysis and design*, pp. 60-81, John Wiley & Sons, 3th edition, 2010.

[36] A. D. Polyanin and V. F. Zaitsev, *Handbook of exact solutions for ordinary differential equations*, Chapman & Hall/CRC Press, Boca Raton, USA, 2003.

The hydriding kinetics of Pd thin films has been investigated in detail. The in-situ experimental technique used in this work consists of a high resolution curvature measurement setup, which continuously monitors the reflections of multiple laser beams reflecting off a cantilevered sample. After mounting the sample inside a vacuum chamber, a H-containing gas mixture is introduced to instantaneously generate a given hydrogen partial pressure (p_{H2}) inside the chamber. The resulting interaction of hydrogen with the Pd layer then leads to a volume expansion of the thin film system. This induces in turn changes in the sample curvature as a result of internal stresses developing in the Pd film during a hydriding cycle. Based on such in-situ curvature data, three different kinetic regimes have been resolved. The first two exhibited a linear increase of the internal stress in the compressive direction with time. A systematic study of the p_{H2}-dependency of the two constant slopes was performed, based on newly derived constitutive kinetic equations. This resulted in the identification of the first linear regime to be limited by absorption and the second one by adsorption. After adsorption equilibrium is reached at the end of the second regime, a third, non-linear kinetic regime, limited by absorption, was found to precede the final hydriding equilibrium. This switch back to absorption-limited kinetics likely occurs due to a coverage dependent change in the adsorption enthalpy of the surface hydrogen. Furthermore, from our in-situ experimental data, relevant kinetic and thermodynamic hydriding parameters have been derived. As a result, this study was able to provide a self-consistent quantitative interpretation of the entire Pd room temperature hydriding cycle in the alpha-phase domain.

The interaction of hydrogen with metals has since long been a topic of scientific and technological interest [1]. In particular, the palladium-hydrogen system has attracted intensive research efforts in physical chemistry as a model system because of its high storage capacity, its high sensitivity and selectivity to H_2 gas, and its ability to easily release hydrogen at room temperature [2]. While for hydrogen-storage materials, intermetallic compounds are nowadays considered to be more promising [3-5], Pd is currently still considered to be a good candidate, especially in thin film form, for applications like hydrogen sensors [6] and gas purification membranes [7]. Additionally, pure Pd is often being used as well in thin film form as a catalytic coating [8].

Despite the model status of the Pd-H system, the exact kinetic details and the rate-limiting step(s) of room temperature Pd hydriding are still a matter of debate [6,9]. As illustrated schematically in Figure 1a, the Pd hydriding mechanism can be divided into four steps. Firstly, gaseous H_2 molecules need to be adsorbed onto the metallic Pd surface. These adsorbed H_2 molecules then dissociate and the resulting H-atoms slip along a minimum energy path towards atomic well positions, from which they can diffuse into the Pd bulk. A Pd hydride is finally formed, with H-atoms mainly occupying the octahedral interstitial sites of the fcc Pd lattice. Consequently, the composition of the palladium hydride is PdH when all bulk sites are occupied. The configuration of those sites is equivalent to the positions occupied by strongly chemisorbed H-atoms on a Pd (111) surface [8]. Depending on the amount of absorbed H, expressed as the bulk H/Pd atomic ratio n, there exist, according to the Pd-H phase diagram, two crystalline Pd-H phases, both keeping the fcc structure of the Pd host [1]: α-PdH, with a relatively low hydrogen solubility ($n_{max}(\alpha)$ = 0.008 at 298 K) and β-PdH, being a non-stoichiometric hydride with $n_{min}(\beta)$ = 0.607 at 298 K. Note that the above-cited room temperature phase stability limits are referring to bulk palladium samples. In the case of Pd nanoparticles, it is now well-established that the miscibility gap becomes narrowed [10,11], while for thin film samples, the film thickness has been reported to have a significant effect as well on the shape of the pressure-concentration isotherms [12]. In fig. 1b, a fifth step in the process is shown, which describes a de-hydriding step in which the hydrogen can be released. This de-hydriding step also illustrates the reversibility of the hydriding process. The kinetics of the whole hydriding/de-hydriding process are spontaneous and reversible.

Determining which of those four kinetic steps in fig. 1a is rate-limiting is typically based on measuring, preferably in-situ, the time-evolution of a H-sensitive parameter with respect to p_{H2}. Such studies have already been reported, based for instance on measurements of Pd cantilever bending [9], optical reflection or transmission [6,13,14], dilatometry [15] and resistivity [16]. However, no consensus on an appropriate kinetic model seems to be available yet, neither qualitatively nor quantitatively. For instance, Hu *et al.* [9] claimed a bending rate of their Pd thin film samples depending on $(p_{H2})^{1/2}$, in agreement with Sievert's law. On the other hand, Zhao *et al.* [6] observed a linear dependence of the hydriding rate with p_{H2} and therefore concluded that the Pd hydriding mechanism was rather controlled by surface interactions.

In this paper, we report on the use of a high resolution curvature measurement technique to perform more accurate quantitative in-situ kinetic studies of Pd hydriding than have previously been reported. Although a few other studies have considered curvature monitoring as well [6,14], none of them have, to the best of our knowledge, been able to reach the same curvature and time resolution as demonstrated in the current paper. This is related to the fact that, unlike current state-of-the-art single-beam curvature measurement techniques, our optical set-up is based on the simultaneous detection of the positions of multiply reflected laser beams into a CCD camera. This has already been shown in a previously published feasibility study to allow for unraveling the kinetics of hydride formation in much more detail [17]. As a result, the presence of different rate-limiting regimes could be recognised for the first time during a single hydriding cycle at constant p_{H2}. In our previous publication [17], these were associated, on a rather speculative basis, with the rate of H-absorption and dissociative H-adsorption, respectively.

The current article extends our initial efforts by systematically studying in-situ the p_{H2} dependence of Pd hydriding, and analysing the results with newly derived constitutive kinetic equations. This will allow for a full interpretation of the hydriding kinetics, including the identification of different rate-limiting steps. Moreover, its quantitative consistency was confirmed by calculating relevant thermodynamic and kinetic hydriding parameters.

Our experimental setup has already been presented in detail in a previous publication [17]. After pumping down a vacuum chamber to base pressures better than 10^{-6} mbar, ultra-pure Ar/H_2 gas mixtures (Alphagaz-grade from Air Liquide) are

introduced into the chamber to instantaneously impose a desired total pressure. The latter is continuously measured by two electronic gauges and one back-up manometer. The compositions of the gas mixtures used in this work are 1% and 100ppm H_2, which allows to further adjust the accessible range of hydrogen partial pressures in the chamber. While hydriding experiments will be reported for p_{H2}

values up to 100 mbar, the quantitative kinetic analysis, which is the main objective of the current paper, has been limited to the low p_{H2} range (2-10 mbar or even 1-10mbar). As will be shown below, this allows to avoid the α to β hydride phase transition, and the sample remains in the α phase (see also fig. 16 for the Pd-H phase diagram). All experiments have been carried out at room temperature.

A high resolution curvature measurement setup, the optical details of which have already been described earlier as well [18] and which is shown in fig. 17, is mounted onto the hydriding chamber. It continuously detects the positions of multiple laser beams reflecting off a cantilevered sample, thus allowing to monitor the sample curvature $\Delta\kappa$ in real time [19]:

$$\Delta\kappa = \frac{\cos\alpha}{2L}\frac{\Delta D}{D_0} \qquad (1)$$

In Eq. (1), $\Delta D/D_o$ is the mean differential spacing between the reflected laser spots in the CCD which change with the curvature of the sample, as is illustrated in fig. 17, L is the distance between the sample and the CCD and α is the angle of laser incidence on the sample. The factor $2L/cos\alpha$ was calibrated as 1.336 m, based on curvature measurements on mirrors with known radius of curvature. As compared to other curvature or deflection measurement techniques, which are generally based on the position detection of a single reflecting laser beam, our set-up has a significantly improved dynamic resolution for the radius of curvature on the order of 10 km, thanks to the noise minimization resulting from the concurrent use of multiple laser beams. Moreover, thanks to the use of a CCD camera, curvature measurements can be performed with a time resolution better than 100 ms. The change in internal stress in the Pd layer, which is simply a result of the prohibited volume change during Pd-H interaction in the thin film geometry as illustrated in fig. 18 for a Pd film on a substrate, can be straightforwardly derived from the measured changes in sample curvature [19]:

$$\Delta\sigma = \frac{1}{6}\frac{E_S}{1-\nu_S}\frac{t_S^2}{t_f}\Delta\kappa \quad (2)$$

with $Y_S=E_S/(1-\nu_S)$ the biaxial elastic modulus of the substrate, and t_S and t_f the substrate and Pd film thickness, respectively. Eq. (2) is the Stoney equation.

The cantilevered samples used for the kinetic analysis were cut approximately 3x0.5 cm^2 in size from oxidized, 425 µm thick Si wafers. These were coated by e-gun evaporation with a Pd thin film, on top of a 5 nm Ti adhesion layer. The purity and thickness of the Pd films were characterized by ICP/OES measurements on layers dissolved in an acid mixture. No contaminant was detected in concentrations exceeding 10 ppb. The Pd thin film thickness, averaged over ten samples from the same wafer, was found to be 128 ± 1 nm. Our Pd thin films were also shown by X-ray diffraction to exhibit a pronounced (111) texture, typical for vacuum deposited fcc metallic thin films [20-22]. Cu Kα radiation was used and the diffractograms were recorded with an angle step of 0.02°. No secondary (200) peak was detected. The texture factor was then calculated using the third peak in terms of standard intensity, resulting in $(I_{(111)}/I_{(311)})_{film}*(I_{(311)}/I_{(111)})_{stand}$ = 38, where the standard intensity ratio $(I_{(111)}/I_{(311)})_{stand}$ was taken from Ref. [23]. The initial growth stress in the as-deposited Pd films, which determines the initial baseline stress level for the hydriding cycle, has been determined as well by recording the sample curvature before and after dissolving the Pd layer from the substrate. Such ex-situ measurements resulted in an average initial tensile growth stress value of 435 ± 3 MPa. Finally, plane-view SEM observations revealed an average grain size of 18 nm. A second batch of Pd films have been deposited under the same conditions in order to perform the experiments that will be reported later to study the hydriding equilibrium. These films had an average thickness of 112 ± 1 nm, an average grain size of 20 nm, a texture factor of 37 and an average initial tensile growth stress of 409 ± 2 MPa, very similar to the films from the other Pd batch.

Fig. 2a shows a typical hydriding cycle performed at p_{H2} = 6 mbar. After an initial baseline curvature measurement in high vacuum, the Ar/H_2 gas mixture was instantaneously introduced in the chamber. As a result of the constrained volume expansion during Pd-H interaction, the internal stress in the Pd thin film increases rapidly in the compressive direction and gradually reaches a constant value. The gas

mixture was then pumped out of the chamber, resulting in a gradual decrease in the internal stress as a result of room temperature dehydriding.

As to the latter, it appears that the internal stress does not go back to its initial value when the gas mixture is pumped out of the vacuum chamber. In other words, a residual hydriding-induced stress is systematically observed when leaving the sample under vacuum after hydriding. In a previous study performed on the same batch of samples [17], a multiple cycling experiment was studied in order to get more insight in this phenomenon. It was shown that this residual stress remains constant from cycle to cycle, even if p_{H2} is changed from one cycle to another. However, the origin of the irreversible part of hydriding under vacuum was not discussed at that stage. An additional single hydriding cycle at p_{H2} = 5.5 mbar is therefore presented in the inset of Fig. 2a and in Fig. 2b, including venting with ambient air after dehydriding in vacuum. It is clearly seen that the residual stress is fully released when the sample is brought into contact with ambient air. This observation indicates that the residual stress observed after dehydriding in vacuum can be attributed to a small residual H-concentration in the Pd lattice, the removal of which can be achieved by venting with air so that a fully reversible hydriding cycle is finally obtained.

From Fig. 2a, two distinct kinetic regimes can be distinguished from the two apparently linear regions of the stress-time curve at the beginning of the hydriding cycle. We believe these two slopes to reveal the presence of different rate-limiting steps in the course of a single hydriding cycle. A third regime is resolved in Fig. 2a as well, characterized by a gradual decrease of the hydriding rate with time until a constant equilibrium stress level is reached. The latter can be associated with chemical equilibrium between atomic H inside the Pd thin film sample and gaseous H_2 available in the chamber. Such a characteristic hydriding behaviour with three distinct kinetic regimes has been observed over the entire p_{H2} interval considered in this paper, and will now be analysed in more detail.

Figure 3 shows the absolute stress levels corresponding to the equilibrium plateau during hydriding experiments up to p_{H2} = 92 mbar. From these results, the α → β phase transition of Pd-hydride can be identified to start at room temperature between 10 and 20 mbar, in agreement with earlier equilibrium hydriding studies on Pd thin films [14]. As a result, the equilibrium stress levels reached in the p_{H2}-range

that will be considered in the present kinetic study (2-10 mbar) correspond to hydrogen concentrations located in the α phase region of the Pd-H system.

For a quantitative kinetic analysis, a link between the bulk H/Pd atomic ratio *n* and the measured internal compressive stress change $\Delta\sigma$ in our Pd thin films needs to be established. This can be done by linking $\Delta\sigma$ to the relative volume change $\Delta V/V$ during hydriding [24]:

$$\Delta\sigma = \frac{E_f}{3(1-\nu_f)}\left(\frac{\Delta V}{V}\right) = \frac{E_f}{3(1-\nu_f)}\left(\frac{\Delta v}{\Omega_{Pd}}\right)n \equiv Q \cdot n \qquad (3)$$

where E_f and ν_f are, respectively, the Young modulus and Poisson ratio of the Pd film. The ratio between $\Delta V/V$ and *n* is equal to $\Delta v/\Omega_{Pd}$, where Δv is the characteristic volume change per hydrogen atom, and Ω_{Pd} is the mean atomic volume of a palladium atom. This ratio, describing the lattice expansion due to hydrogen uptake, has been the object of many studies in the past, from which a value of 0.19 ± 0.01 can be derived [25]. Eq. (3) then enables to link the measured hydriding-induced internal stress changes $\Delta\sigma$ to the bulk H/Pd atomic ratio *n* via some mechano-physical constants, which for convenience are grouped together into a single proportionality factor *Q*.

It should be noted that a possible complicating factor in Eq. (3) is the occurrence of an α to β phase transformation during Pd hydriding, each having their own characteristic lattice expansion behaviour so that the measured stress change will depend on the exact proportions of the α and β phases. Although the value of 0.19 has been suggested by Peisl for the whole compositional range in the Pd-H system, the collected data are too scarce to state that there is no effect of the α to β phase transformation on the lattice expansion. However, as already indicated with Fig. 3, this complicating factor does not need to be dealt with in the present study because the α to β phase transformation is avoided by limiting the p_{H2}-range.

Eq. (3) also makes the explicit assumption that the deformation resulting from the hydriding-induced internal stress is elastic [26]. Thanks to the relatively high initial tensile growth stress of our as-deposited Pd films, and the fact that the kinetic studies have been limited to the α phase region, this condition has been verified as well. In Fig. 2a for instance, it is seen that the equilibrium compressive stress change of this cycle is about 435 MPa. Taking into account the initial tensile growth stress level of 435 MPa in the as-deposited Pd film, this leads to an almost zero equilibrium stress value. Similarly, Fig. 3 shows that, over the entire α phase region,

the maximum absolute value of the equilibrium stress level is smaller than 200 MPa, therefore well below the Pd theoretical yield stress [27]. Plastic deformation of our Pd thin films during hydriding in the α phase region can therefore be reasonably excluded. As a result, the time derivative of the hydriding curves obtained experimentally can be considered as directly proportional to the hydriding velocity dn/dt. We can point out as well that these observations also confirm our earlier finding that the residual stress observed in Fig. 2a after dehydriding in vacuum can be attributed to a small residual H-concentration in the Pd lattice.

Based on the above considerations, we can already use Eq. (3) to determine Sievert's constant K_s from our experimentally determined equilibrium stress data in the α phase region of Fig. 3. Indeed, when linearising these data as a function of $(p_{H2})^{1/2}$, according to Sievert's law in α-PdH [1]:

$$(\Delta\sigma)_{eq} = Q \cdot n_{eq} = Q \cdot \frac{\sqrt{p_{H_2}}}{K_s} \qquad (4)$$

with n_{eq} the equilibrium atomic hydrogen concentration in the bulk. The slope of the linear fit shown in Figure 4 yields a K_s value of 3.3 ± 0.7 atm$^{1/2}$ (using E_{Pd} = 121 GPa and ν_{Pd} = 0.39 [28]). Room temperature K_s values for Pd hydriding have been reported in a rigorous study by Bucur [29] to be in the range 2-20 atm$^{1/2}$, the higher value corresponding to a perfect crystal structure (i.e. well-annealed bulk palladium samples) and the lower one corresponding to a relatively large concentration of structural defects, typical for as-evaporated thin Pd films [29]. Our own value is therefore in excellent agreement with the data from Bucur, recognising that our evaporated Pd thin films probably contain a large defect concentration as well resulting from the deposition process. Since the defect concentration and the mean internal stress are related, Sievert's constant depends on the internal stress, as illustrated for our samples in fig. 24.

Following our previously reported hydriding study at fixed p_{H2} [17], we will consider the possibility of 2 mechanistic steps to be rate-limiting during Pd thin film hydriding. One of these steps includes H_2 adsorption and its dissociative chemisorption on the Pd thin film surface, and will conveniently be called adsorption. The other one, denoted as absorption, is seen as an equilibrium reaction between atomic hydrogen at, respectively, the surface sites and the interstitial sites

of the Pd hydride. In his classical hydriding model, Wagner wrote down the following reactions to describe each of these steps [1]:

$$H_2 + 2s \Leftrightarrow 2H - s \quad (5)$$

$$H - s + i \Leftrightarrow H - i + s \quad (6)$$

where *s* and *i* are a free surface adsorption site and an interstitial bulk absorption site, respectively, while *H-s* and *H-i* represent, respectively, a surface and bulk site occupied by atomic H.

More rigorously, earlier studies claimed the existence of two possible adsorption sites on the Pd (111) surface [1]: the so-called strong and weak adsorption sites, which correspond to, respectively, very deep and rather flat potential wells. The strong adsorption sites are octahedral sites, also called fcc sites [8]. Despite the existence of three other highly exothermic surface sites (called bridge, top and hcp sites), it has been claimed that only the fcc sites need to be taken into account for strong chemisorption on (111) planes of Pd. As indeed suggested by Bucur in one of his thin film hydriding models [30], the strong adsorption sites are filled well before and much faster than the weak ones.

More recently, Johansson *et al.* obtained accurate computational data for the heat of adsorption on Pd (111) surfaces [31]. The heat of adsorption starts from about -100 kJ/mol H_2 at zero surface coverage θ, θ being the number of adsorbed hydrogen atoms divided by the number of adsorbed hydrogen atoms in a filled monolayer. It then gradually becomes less negative as θ increases, and rather abruptly takes on positive values somewhere in the range $0.75 < \theta < 1$. This result clearly suggests a more complex adsorption behavior than the one proposed by Bucur. Hong and Rahman arrived at a similar conclusion in their first-principles electronic structure calculations [32], showing that it is only after a substantial amount of hydrogen is adsorbed on the Pd (111) surface that hydrogen is able to further absorb into the bulk. Similarly, the potential energy surface for hydrogen adsorption/absorption [33] also indicates that a surface that is already substantially covered with hydrogen helps the hydrogen atoms to overcome the energy barrier to move into the bulk.

With respect to the schematics of Fig. 1a, no hydrogen diffusion step will be taken into account in the present kinetic model, simply because of the Pd thin film geometry considered in our work. Indeed, one gets a first-order diffusion time on

the order of milliseconds when dividing the square of the Pd film thickness by the diffusion coefficient of H-atoms in α-PdH ($D_\alpha \cong 10^{-7}$ cm^2/s [6]). This is five orders of magnitude below the time scale of the hydriding kinetics experimentally observed in Fig. 2a for our Pd thin films.

As to the adsorption step, described by reaction (5), an adsorption equilibrium constant K_{ad} can be defined as follows:

$$K_{ad} \equiv \frac{k_{ad}^{'}}{k_{ad}^{''}} = \frac{[H-s]_{eq}^2}{p_{H_2}[s]_{eq}^2} = \frac{\theta_{eq}^2}{(1-\theta_{eq})^2}\frac{1}{p_{H_2}} \qquad (7)$$

where θ_{eq} is the equilibrium surface coverage. From reaction (5), the adsorption velocity r_{ad} then takes on the following form [34] :

$$r_{ad} = k_{ad}^{'}(1-\theta)^2 p_{H_2} - k_{ad}^{''}\theta^2 = k_{ad}^{'}\left[(1-\theta)^2 p_{H_2} - \frac{\theta^2}{K_{ad}}\right] \qquad (8)$$

In a similar way, the absorption equilibrium constant K_{ab} can be deduced from reaction (6):

$$K_{ab} \equiv \frac{k_{ab}^{'}}{k_{ab}^{''}} = \frac{[H-i]_{eq}[s]_{eq}}{[H-s]_{eq}[i]_{eq}} = \frac{1-\theta_{eq}}{\theta_{eq}} \cdot \frac{n_{eq}}{1-n_{eq}} \qquad (9)$$

Note that the equilibrium constants K_{ad} and K_{ab} can be linked together with Sievert's constant by grouping Eqs. (4), (7) and (9), and by assuming that $n_{eq} << 1$ in α-PdH:

$$K_{ad} \cdot K_{ab}^2 = \frac{1}{K_S^2} \qquad (10)$$

From reaction (6), the absorption velocity r_{ab} can then be written as:

$$r_{ab} = k_{ab}^{'}(1-n)\theta - k_{ab}^{''}n(1-\theta) = k_{ab}^{'}\left[(1-n)\theta - \frac{n(1-\theta)}{K_{ab}}\right] \qquad (11)$$

Finally, the evolution of the surface coverage θ and bulk H/Pd atomic ratio n can then be deduced by combining the expressions (8) and (11) for the ad- and absorption velocities :

$$\frac{d\theta}{dt} = 2r_{ad} - r_{ab} \tag{12}$$

$$\frac{dn}{dt} = r_{ab} \tag{13}$$

When dealing with complex second order reactions as is the case here, the derivation of general rate expressions taking into account each of the two reaction steps is exceedingly tedious or even impossible to derive. The common alternative method in chemical kinetics then consists in assuming a specific rate-controlling step right from the beginning, and considering the other reaction step to be in a pseudo steady-state [35]. In our case, if we assume that the two constant slopes observed in Fig. 2a during the first and second kinetic regimes reveal the presence of two different rate-limiting steps, we can then derive simplified expressions for the adsorption and absorption velocities by assuming that, respectively, the absorption or adsorption step is in pseudo steady-state.

Let us first assume that adsorption is the rate-limiting step. In that case, we can consider $k'_{ab} \rightarrow \infty$, and as r_{ab} must remain finite according to Eq. (11) [35], this leads to $(1-n)\theta - n(1-\theta)/K_{ab} \rightarrow 0$, that is to say:

$$\theta = \frac{1}{1 + K_{ab}\dfrac{1-n}{n}} \cong \frac{n}{n + K_{ab}} \tag{14}$$

This equation then enables to eliminate the unobservable variable θ, since in our experimental approach based on assessing hydriding-induced volume changes, we are only able to access the bulk H/Pd atomic ratio n and not the surface coverage θ (cfr. eq. (3)). Inserting Eq. (14) into Eq. (8) finally gives:

$$r_{ad} = k'_{ad}\left[p_{H_2}\left(\frac{K_{ab}}{K_{ab}+n}\right)^2 - \frac{1}{K_{ad}}\left(\frac{n}{K_{ab}+n}\right)^2 \right] \tag{15}$$

On the other hand, if it is assumed that absorption is the rate-limiting step, one can write $k'_{ad} \rightarrow \infty$ so that from Eq. (8), similarly as in the reasoning above, $p_{H2}(1-\theta)^2 - \theta^2/K_{ad} \rightarrow 0$. This equation then leads to the following solution for the pseudo steady-state surface coverage θ :

$$\theta = \frac{\sqrt{p_{H2}K_{ad}}}{1+\sqrt{p_{H2}K_{ad}}} \qquad (16)$$

Inserting Eq. (16) into Eq. (11) finally gives:

$$r_{ab} = k'_{ab}\left[\frac{K_{ab}(1-n)\sqrt{p_{H_2}K_{ad}} - n}{K_{ab}(1+\sqrt{p_{H_2}K_{ad}})}\right] \qquad (17)$$

Note that equations (15) and (17), predicting the p_{H2}-dependences of the adsorption and absorption velocities, have been derived while explicitly assuming $n << 1$. This is indeed the case for the range of p_{H2}-values considered in the present work for room temperature hydriding in the alpha phase region ($n_{max}(a)$ = 0.008 in bulk Pd).

After recognising the existence of 2 possible rate-controlling reaction steps, one can reasonably assume, as a starting point for a rigorous kinetic analysis, that the two constant slopes that are systematically observed in the beginning of our hydriding cycles (cfr. Fig. 2a) would correspond to a different kinetic regime, with either ad- or absorption being the rate-limiting step. Since at the beginning of the experiment (when θ = 0 and n = 0) the adsorption velocity has already a finite value (cfr. eq. (8)) while the absorption velocity is still 0 (cfr. eq. (11), and since adsorption can be considered as relatively unconstrained on a freshly exposed surface, one could reasonably imagine that the first linear kinetic regime corresponds to an absorption-limited step. The second slope would then be indicative for adsorption to become rate-controlling further on in the hydriding cycle. In order to confirm this assumption, a systematic study of the p_{H2}-dependence of the measured constant slopes was first carried out.

According to eq. (3), these slopes can be taken proportional to $(dn/dt)_{ab}$ and $(dn/dt)_{ad}$ in each of the 2 "linear" kinetic regimes, respectively. Constitutive equations for these quantities therefore still need to be derived first. As to $(dn/dt)_{ab} \equiv r_{ab}$ (cfr. eq. (13)), Eq. (17) can be further simplified with the additional

assumption that $p_{H2} \cdot K_{ad} >> 1$. At this stage, the latter can be justified from Eq. (7), since, from the state-of-the-art discussion above, the equilibrium surface coverage can be considered to be close to one. We will be able to explicitly verify this assumption later in this work, based on derived values for K_{ad}. Combining Eq. (17) with Eqs. (10) and (13) then gives

$$\left(\frac{dn}{dt}\right)_{ab} = k'_{ab}\left[(1-n) - \frac{K_S n}{\sqrt{p_{H_2}}}\right] \qquad (18)$$

An absorption-limited hydriding mechanism can therefore be expected to exhibit a hydriding velocity proportional to $(p_{H2})^{-½}$.

The slope $(dn/dt)_{ad}$ of the second linear regime can be derived by linking the differentials of the surface coverage θ and bulk H/Pd atomic ratio n thanks to Eq. (14), resulting in $d\theta = (K_{ab}/(K_{ab}+n)^2) \cdot dn$. Combining Eq. (15) with Eqs. (10), (12) and (13) then provides

$$\left(\frac{dn}{dt}\right)_{ad} = \frac{2k'_{ad}K_{ab}^2}{\left(K_{ab}+n\right)^2 + K_{ab}}\left[p_{H_2} - \left(K_S n\right)^2\right] \qquad (19)$$

indicating that an adsorption-limited hydriding mechanism exhibits a hydriding velocity which can be expected to increase linearly with p_{H2}.

In Figures 5a and 5b, the slopes of the first linear kinetic regime have been plotted as a function of $1/(p_{H2})^{½}$, following constitutive Eq. (18) for an absorption-limited hydriding velocity. Figure 5b clearly shows the effect of mechanical stress on the first kinetic regime (the absorption kinetics are effected by mechanical stress). Similarly, Figures 6a and 6b show the slopes of the second linear regime, which exhibit a linear relationship with p_{H2}, in agreement with Eq. (19). Figure 6b shows that there no clear effect in the studied samples of the mechanical stress on the second kinetic regime (the adsorption kinetics are largely unaffected by mechanical stress). All these figures therefore provide additional, although still qualitative, experimental evidence that the first kinetic hydriding regime is indeed likely to be limited by absorption and the second one by adsorption. It has to be recognised though that, although the p_{H2} dependencies shown in Figs. (5a), (5b), (6a) and (6b) are consistent with our kinetic interpretation, the same graphs would still look more

or less linear when claiming other reaction orders, like proportional with p_{H2} for Fig. 5a and 5b or proportional to $1/(p_{H2})^{1/2}$ for Fig. 6a and 6b. Therefore, if one defines, respectively, S_{ab} and S_{ad} as the slopes and I_{ab} and I_{ad} as the intercepts of the claimed linear fits in Fig. 5a and 6a, these parameters should as such also result in quantitatively relevant kinetic and thermodynamic hydriding parameters. This can be verified based on the following expressions:

$$\frac{S_{ad}}{Q} = \frac{2k'_{ad}K_{ab}^2}{(K_{ab}+n)^2 + K_{ab}} \tag{20}$$

$$\frac{I_{ad}}{Q} = \frac{-2k'_{ad}K_{ab}^2}{(K_{ab}+n)^2 + K_{ab}} \cdot (K_S n)^2 \tag{21}$$

$$\frac{S_{ab}}{Q} = -k'_{ab}K_S n \tag{22}$$

$$\frac{I_{ab}}{Q} = k'_{ab}(1-n) \tag{23}$$

Note that the proportionality constant Q has already been introduced before with Eq. (3) in order to convert the measured velocities $(dn/dt)_{ad/ab}$ (expressed in s^{-1}) to the units of the data points in Figs. 5a and 6a (expressed in MPa/s). The evolution of the absorption rate constant $k'_{ab,I}$ in the first kinetic regime with the hydrogen partial pressure and its dependence on the mechanical stress is illustrated in fig. 22. From Eqs. (20-23), it is clear that S_{ad} and I_{ab} should be positive, while S_{ab} and I_{ad} should be negative. This is indeed observed in the experimental fits obtained in Figs. 5a and 6a. Before trying to solve the 4-equation system involving Eqs. (20-23), one can first define a time t_{tr} to indicate the transition between the first and second kinetic regime. As indicated in the inset of Figure 7, this time should respect the following geometrical relationship:

$$\left[\left(\frac{dn}{dt}\right)_{ad}\Big|_{t=t_{tr}}\right] \cdot t_{tr} - \frac{I_\sigma}{Q} = \left[\left(\frac{dn}{dt}\right)_{ab}\Big|_{t=t_{tr}}\right] \cdot t_{tr} \tag{24}$$

where I_σ is the intercept of the linear fit through the second kinetic regime relative to the initial, as-deposited growth stress value (cfr. inset of Fig. 7). The latter

parameter has been determined experimentally for all hydriding experiments, resulting in an average value of 446 ± 27 MPa, independent of p_{H2} in the range 2-10 mbar considered here (cfr. supporting information). By combining Eqs. (20-23) with Eq. (24), we obtain

$$t_{tr} = \frac{I_\sigma}{(S_{ad} p_{H_2} - S_{ab} \frac{1}{\sqrt{p_{H_2}}} + I_{ad} - I_{ab})} \quad (25)$$

Figure 7 shows the experimental transition times, determined from the intersection of the linear fits in the first and second kinetic regime, as well as their p_{H2}-dependence predicted by Eq. (25). For the latter, the S_i and I_i values were taken from the linear fits of Figs. 5 and 6. The excellent correlation obtained between the predicted and experimental t_{tr} values confirms that our kinetic model makes sense, both qualitatively and quantitatively.

The 4-equation system involving Eqs. (20-23) then provides a first access to some relevant kinetic and thermodynamic parameters, simply by dividing the slope and intercept values corresponding to the ad- and absorption limited regime:

$$\frac{S_{ad}}{I_{ad}} = -\frac{1}{(K_S n)^2} \quad (26)$$

$$\frac{S_{ab}}{I_{ab}} = -K_S \cdot \frac{n}{1-n} \quad (27)$$

Since we already determined the value of Sievert's constant K_s (cfr. Fig. 4), Eq. (26) gives a calculated average value for n of $(1.3 \pm 0.3)\cdot 10^{-2}$ for the second, adsorption-limited kinetic regime, while Eq. (27) results in a calculated average n-value of $(1.4 \pm 0.4)\cdot 10^{-2}$ for the first, absorption-limited regime. These average values can indeed be considered to be sufficiently small in order for Eqs. (18) and (19) to result in the seemingly constant slopes observed in the first and second kinetic regimes. Moreover, its implication that n at $t = t_{tr}$ is independent of p_{H2} is not surprising if one considers the constant compressive stress level of our samples at $t = t_{tr}$, which was found to be - 94 ± 6 MPa relative to the initial, as-deposited growth stress value, independent of p_{H2} (cfr. supporting information).

As we now explicitly confirmed that $n << 1$ in this work, Eq. (23) immediately results in $k'_{ab} = (7.4 \pm 0.8)\cdot 10^{-5}\ s^{-1}$ for the first regime. When taking $k''_{ab} = 1\cdot 10^{9}\ s^{-1}$, calculated at 298.15 K from Ref. [33], and knowing that $K_{ab} \equiv k'_{ab}/\ k''_{ab}$, we obtain a value of $K_{ab} = (7.4 \pm 0.8)\cdot 10^{-14}$, and therefore $K_{ad} = (1.6 \pm 0.8)\cdot 10^{22}\ mbar^{-1}$ from Eq. (10). The latter therefore also validates our earlier hypothesis of $p_{H2}\cdot K_{ad} >> 1$,

needed for arriving at eq. (18). Moreover, inserting the calculated K_{ab} value and the previously obtained value of n into Eq. (20) gives $k'_{ad} = (5 \pm 3)\cdot 10^{17}\ mbar^{-1}s^{-1}$. As a value of K_{ad} has already been derived, and since $K_{ad} \equiv k'_{ad}/\ k''_{ad}$, one also arrives at $k''_{ad} = (3 \pm 2)\cdot 10^{-5}\ s^{-1}$, in good agreement with the value of $k''_{ad} = 6.9\cdot 10^{-5}\ s^{-1}$ calculated at 298.15 K from Ref. [33].

Besides the presence of the two linear kinetic regimes analysed above, a third non-linear regime was resolved in Fig. 2a as well to precede the final hydriding equilibrium. Fig. 8 shows, for different p_{H2}-values, the evolution of the bulk hydrogen concentration in this third kinetic regime, as calculated from the internal stress data using Eq. (3). The time scale has been normalised to represent for each experiment the first 500 s of this regime. If we assume that absorption is the rate-limiting step in this regime, the temporal evolution of n can be deduced from Eq. (18) by solving what is known as a basic Cauchy problem [36]:

$$\begin{cases} \dfrac{dn(t)}{dt} = n(t)\cdot C_1 + C_2 \\ n(t_0) = n_0 \end{cases} \qquad (28)$$

where t_0 refers to the transition time between the second and third kinetic regime, and

$$\begin{cases} C_1 = -k'_{ab}\left(1 + \dfrac{K_S}{\sqrt{p_{H_2}}}\right) \\ C_2 = k'_{ab} \end{cases} \qquad (29)$$

The general solution of this problem is as follows [36]:

$$n(t) = \frac{-C_2}{C_1} + \left(n_0 + \frac{C_2}{C_1} \right) \exp\left(C_1 (t - t_0)\right) \qquad (30)$$

The coarse solid lines in Fig. 8 correspond to the fits obtained with the absorption-related Eq. (30). Intuitively, it can be understood that the third kinetic regime must indeed be limited by absorption because at the end of the second regime, the surface coverage has already reached its equilibrium value. In this case, the constant C_2 in Eq. (29) then directly provides an estimate for k'_{ab}.

The thus obtained average value of C_2 for all experiments, calculated from fitting eq. (30) to the third kinetic regime, results in an average value of $k'_{ab} = (4.1 \pm 0.9) \cdot 10^{-4}\ s^{-1}$ for the third kinetic regime. Moreover, when repeating this procedure for the first kinetic regime, one gets $k'_{ab} = (3.3 \pm 0.8) \cdot 10^{-5}\ s^{-1}$, consistent with the value of $k'_{ab} = (7.4 \pm 0.8) \cdot 10^{-5}\ s^{-1}$ previously obtained with the approximate eq. (23). The value of k'_{ab} for the first kinetic regime is however about one order of magnitude lower than the one characteristic for the third kinetic regime. Therefore, the major outcome of our kinetic study is that the absorption-controlled regimes I and III are characterised by very different values for k'_{ab}. In our opinion, this is related to the fact that the end of region I is being determined by a rather abrupt increase in the positive direction of the heat of adsorption. This is in line with ref. [31], where such an increase was reported to occur somewhere in the range $0.75 < \theta < 1$. In that case, k'_{ab} must increase as well since the potential energy surface for hydrogen adsorption/absorption indicates that the activation energy for hydrogen absorption should decrease if the heat of adsorption becomes less negative [33]. In this respect, we can also point out that the factor of 10 difference observed between k'_{ab} in regions 1 and 3 implies a coverage dependent change in activation energy on the order of RT.ln(10), corresponding to 6 kJ/molK at 298 K. This number can indeed be considered to be a realistic change for a coverage dependant heat of adsorption, and is within the range of coverage dependence published for Pd surfaces [31].

As a summary, Figure 9 schematically represents the evolution of the adsorption and absorption velocities as a function of surface coverage, as can be anticipated from the current kinetic study. The velocities are superimposed on the experimentally measured hydriding cycle already shown in Fig. 2a. The latter has also been simulated/fitted according to eq. (30) and (19). According to Eq. (8), the

θ-dependency of the adsorption velocity is a decreasing parabola, while, according to Eq. (11), the absorption velocity increases linearly with θ. In the beginning of the experiment, the initial adsorption and absorption velocities are, respectively, $r_{ad} = k'_{ad} \cdot p_{H2}$ and $r_{ab} = 0$. In the first linear kinetic regime, r_{ad} then rapidly decreases as θ reaches a value close to θ_{eq}. In this zone, Eq. (11) predicts the rate-limiting absorption velocity dn/dt to increase linearly with θ and to decrease linearly with n, which is probably the reason why a constant average velocity is observed experimentally. When a critical value of the surface coverage is reached at the end of the first kinetic regime (denoted θ_c in Fig. 9), the heat of adsorption is believed to suddenly change in the positive direction. This is illustrated in fig. 21, which also shows the decrease of the heat of adsorption caused by the mechanical stress on the film. As a result, adsorption then becomes the new rate-limiting step, and the second kinetic regime starts. In this second zone, a plausible explanation for the observation of a constant average velocity is the fact that an increase in θ implies an increase in dn/dt. The increase of surface coverage is thus counterbalanced by the increasing absorption velocity, so that the apparent rate-limiting velocity appears as constant until adsorption equilibrium is reached. When the latter occurs at the end of the second stage ($\theta = \theta_{eq}$), the absorption velocity becomes rate-limiting again in the third kinetic regime. In fig. 23, one can see how applying mechanical stress may improve the activation volume for hydrogen absorption. In this regime, dn/dt decreases with n and the kinetics are not linear anymore (cfr. Eq. (30)). An equilibrium stress plateau finally appears when absorption equilibrium is reached ($n = n_{eq}$).

Finally, Table 1 shows all the relevant kinetic and thermodynamic parameters calculated in this work, as well as the kinetic regimes to which they apply. Some literature values are also included, like the constant k''_{ab} that we used in this study for some of the related calculations. Other reference values from the literature show the overall consistency of the obtained results.

Table 1:

Overview of the kinetic and thermodynamic hydriding parameters calculated in this work for Pd hydriding in the α phase region at 298K, with the kinetic regimes which they apply to. Some values taken from the literature are displayed for comparison.

Parameter	Origin	1st regime	2nd regime	3rd regime	Overall
k'_{ad} [$mbar^{-1}s^{-1}$]	This work		$(5 \pm 3)\cdot10^{17}$		
k''_{ad} [s^{-1}]	This work		$(3 \pm 2)\cdot10^{-5}$		
	Ref. [33]				$6.9\cdot10^{-5}$
K_{ad} [$mbar^{-1}$]	This work				$(1.6 \pm 0.8)\cdot10^{22}$
k'_{ab} [s^{-1}]	This work	$(7.4 \pm 0.8)\cdot10^{-5}$	$(4.1 \pm 0.9)\cdot10^{-4}$	$(4.1 \pm 0.9)\cdot10^{-4}$	
k''_{ab} [s^{-1}]	Ref. [33]				$1\cdot10^{9}$
K_{ab} [-]	This work				$(7.4 \pm 0.8)\cdot10^{-14}$
K_s [$atm^{1/2}$]	This work				3.3 ± 0.7
	Ref. [29]				2

A new in-situ diagnostic tool, based on the real-time monitoring of hydriding-induced internal stresses, has been used for the in-situ study of the hydriding kinetics of Pd thin films. Three different kinetic regimes have been resolved. The first two exhibited a linear increase of the internal stress in the compressive direction with time. A systematic study of the p_{H2}-dependency of these two constant slopes, based on newly derived constitutive equations, resulted in the identification of the first linear regime to be limited by absorption and the second one by adsorption. After adsorption equilibrium is reached at the end of the second stage, a third, non-linear kinetic regime, limited by absorption, was found to preceed the final equilibrium. The quantitative analysis of these different regimes resulted in the calculation of a number of relevant kinetic and thermodynamic hydriding parameters. One of the major outcomes in this respect is that the rate constant for hydrogen absorption k'_{ab} in the first and third kinetic regimes differ by almost one order of magnitude. This has been attributed to the fact that the end of the first regime is being determined by a rather abrupt increase in the positive direction of the heat of adsorption. As a result, this study was able to provide a self-consistent quantitative interpretation of the entire room temperature Pd hydriding cycle in the α-phase domain.

<u>Study B: effect of internal stress on the hydriding kinetics of nanocrystalline Pd thin films</u>

A further study of the effect of internal stress on the hydriding kinetics of nanocrystalline Pd thin films was conducted and is described below. In what follows, reference is made to the following publications:

[1] von Pezold J, Lymperakis L, Neugebeauer J. Acta Mater 2011;59:2969.
[2] Birnbaum HK, Sofronis P. Mater Sci Eng A 1994;176:191.
[3] Song J, Curtin WA. Acta Mater 2011;59:1557.
[4] Flanagan TB, Mason NB, Birnbaum HK. Scr Metall 1981;15:109.
[5] Wagner S, Pundt A. Acta Mater 2011;59:1862.
[6] Wagner S, Pundt A. Appl Phys Lett 2008;92:051914.
[7] Baldi A, Gonzalez-Silveira M, Palmisano V, Dam B, Griessen R. Phys Rev Lett 2009;102:226102.
[8] Gremaud R, Gonzalez-Silveira M, Pivak Y, de Man S, Slaman M, Schreuders H, Dam B, Griessen R. Acta Mater 2009;57:1209.
[9] Yamamoto K, Orimo S, Fujii H, Kitano Y. J Alloys Compd 1999;293-295:546.
[10] Bobet JL, Chevalier B, Darriet B. J Alloys Compd 2002;330:738.
[11] Bobet JL, Chevalier B, Song MY, Darriet B, Etourneau J. J Alloys Compd 2002;336:292.
[12] Wicke E, Brodowsky H. Hydrogen in palladium and palladium alloys, in: Alefeld G, Voelkl J (Eds.). Hydrogen in metals, vol. 2. Berlin: Springer; 1978.
[13] Lewis FA. The palladium hydrogen system. London: Academic Press; 1967.
[14] Fleischer EL. MRS Bull 2002;27(9):675.
[15] Chen P, Zhu M. Mater Today 2008;11:36.
[16] Jones RH, Thomas G. JOM 2007;59:50.
[17] Zhao Z, Sevryugina Y, Carpenter MA, Welch D, Xia H. Anal Chem 2004;76:6321.
[18] Kulprathipanja A, Alptekin GO, Falconer JL, Way JD. J Membr Sci 2005;254:49.
[19] Jewell JJ, Davis BH. Appl Catal A 2006;310:1.
[20] Delmelle R, Bamba G, Proost J. Int J Hydrogen Energy 2010;35:9888.
[21] Proost J, Spaepen F. J Appl Phys 2002;91:204.
[22] Van Overmeere Q, Vanhumbeeck JF, Proost J. Rev Sci Instrum 2010;81:045106.
[23] Delmelle R, Proost J. Phys Chem Chem Phys 2011;13:11412.
[24] Smithells CJ. Metals Reference Book, eighth ed. London: Butterworths; 2004.
[25] Thornton JA. J Vac Sci Technol 1974;11:666.
[26] Thornton JA, Tabock J, Hoffman DW. Thin Solid Films 1979;64:111.
[27] Floro JA, Hearne SJ, Hunter JA, Kotula P, Chason E, Seel SC, Thompson CV. J Appl Phys 2001;89:4886.
[28] Kuru Y, Wohlschlögel M, Welzel U, Mittemeijer EJ. Surf Coat Technol 2008;202:2306.

[29] Joshi N, Aswal DK, Debnath AK, Gupta SK, Yakhmi JV. Appl Surf Sci 2004;228:302.
[30] Singh U, Jha N, Singh TP, Kapoor A, Perrone A. Opt Laser Technol 2010;42:1128.
[31] Kern A, Eysel W. Mineralogisch-Petrograph. Inst. Univ. Heidelberg, Germany, ICDD Grant-in-Aid; 1993.
[32] Sanders PG, Eastman JA, Weertman JR. Acta Mater 1997;45:4019.
[33] Youngdahl CJ, Sanders PG, Eastman JA, Weertman JR. Scripta Mater 1997;37:809.
[34] Peisl H. Lattice strains due to hydrogen in metals, in: Alefeld G, Voelkl J (Eds.). Hydrogen in metals, vol. 1. Berlin: Springer; 1978.
[35] Bucur RV. J Mat Sci 1987;22:3402.
[36] Froment GG, Bischoff KB, DeWilde J. Chemical reactor analysis and design, third ed. Hoboken: Wiley; 2010.
[37] Johansson M, Skúlason E, Nielsen G, Murphy S, Nielsen RM, Chorkendorff I. Surf Sci 2010;604:718.
[38] Polyanin AD, Zaitsev VF. Handbook of exact solutions for ordinary differential equations. Boca Raton: Chapman & Hall/CRC Press; 2003.
[39] Ward TL, Dao T. J Membr Sci 1999;153:211.
[40] Mejdell AL, Chen D, Peters TA, Bredesen R, Venvik HJ. J Membr Sci 2010;350:371.
[41] Wang HC, Baltruschat H. ChemPhysChem 2010;11:2798.
[42] White JR. J Mat Sci 1981;16:3249.
[43] Hong S, Rahman TS. Phys Rev B 2007;75:155405.
[44] Baranowski B, Majorowski S. J Less Common Met 1984;98:L27.

Internal stresses are a key issue in the design of materials that interact with hydrogen, for instance for sensing or storage applications. While an increasing amount of evidence in the literature points to an effect of internal stress on the equilibrium H-uptake, it is still an open question to what extent the hydriding kinetics can be stress-affected as well. This is the main objective of the current paper, using nanocrystalline Pd thin films with varying degrees of growth-induced internal stress levels as a model system. The key experimental technique used consists of a high resolution curvature measurement setup. After mounting the sample inside a high vacuum chamber, a H-containing gas mixture is introduced to instantaneously generate a given hydrogen partial pressure (pH2) inside the

chamber. The resulting interaction of H with the Pd layer then leads to a prohibited volume expansion of the thin film system, inducing in turn changes in the sample curvature. Such curvature data, obtained in-situ at different pH2, have first been interpreted with a self-consistent kinetic model in order to identify the different rate-limiting steps during a hydriding cycle. Next, the corresponding rate constants have been calculated, as well as their variation with internal stress. It was found that internal stress does not affect the rate constant of the adsorption-limited regime in the range 60-450 MPa, leading to an average value of (1.1 ± 0.2) $mbar^{-1}s^{-1}$ over the experimentally covered p_{H2} range 1-10 mbar. As to the absorption-limited regime, a significant stress effect was recorded on the absorption rate constant of the very initial stages of hydriding, leading to an activation volume of 17.6 ± 2.3 $Å^3$ for H-absorption into our Pd thin films. This value, combined with an internal tensile stress on the order of 450 MPa in our nanocrystalline Pd films, leads to a decrease of the activation energy for H-absorption of 3 kJ/mol. This effect induces up to a factor 3 increase in the room-temperature absorption rate in the initial stages of hydriding.

Although often considered as an undesirable source of embrittlement in metallic alloys, the interaction between hydrogen and metals has also been widely studied for applications like gas purification membranes and hydrogen storage or sensor systems. In the field of hydrogen embrittlement in metals, fracture mechanisms involve accumulation of hydrogen atoms in the local tensile strain field around dislocations and crack tips, either invoking hydrogen-enhanced local plasticity (HELP) [1,2] or hydride formation and cleavage [3,4]. In these mechanisms, distortion of the host metal matrix caused by a local tensile strain field favors hydrogen accumulation in the available lattice sites as well as the formation of hydrogen trapping sites. In the case of HELP, H forms Cottrell atmospheres around dislocation cores and in the case of hydride formation and cleavage, brittle hydrides grow around dislocations, possibly leading to the formation of micro-cracks even at dilute bulk H-concentrations. Similar relationships between the mechanism of hydrogen uptake and the stress/strain state of the host metallic lattice are of primary importance as well in hydrogen sensors, membranes or storage applications. In these systems, an effect of internal stress on the hydriding thermodynamics has been reported for both thin films [5-8] and powders [9-11]. In

thin films, internal stress can be generated in different ways, like clamping metallic layers and using different types of substrates [5], using layers partially or totally

detached from their substrates [6], and through elastic constraints using sandwiched metallic layers [7]. In powders, the stress-related parameter is usually the milling time, for which an optimum exists, claimed to correspond to a state of the maximum internal stress [10,11]. The above studies provide clear evidence that both global and local internal stresses can have a non-negligible effect on the equilibrium hydriding behavior of metallic compounds, affecting thermodynamic parameters like equilibrium H-uptake and miscibility gaps [6,7]. On the other hand, a possible effect of internal stress on the kinetics of hydriding has to the best of our knowledge not been considered so far. This is the main objective of the current paper.

Among the metals of which the interaction with hydrogen has since long been a topic of scientific and technological interest [12], the palladium–hydrogen system

has particularly attracted intensive research efforts as a model system because of its high storage capacity, its high sensitivity and selectivity to H_2 gas, and its ability to easily release hydrogen at room temperature [13]. For hydrogen-storage materials, other inorganic compounds are nowadays considered to be more promising [14–16]. However, Pd is currently still being considered to be a good candidate for applications like hydrogen sensors [17] and gas purification membranes [18], especially in thin film form. Additionally, pure Pd is often being used as well as a catalytic coating [19].

In this study, a high-resolution in-situ curvature measurement set-up [20] has been used on model Pd thin films for two purposes. Firstly, it allowed to measure in-situ the evolution of the growth-induced internal stress in our Pd thin films during deposition. Secondly, it was then also used to study the hydriding kinetics of these Pd thin films, allowing to unravel each kinetic regime in quantitative detail. Firstly, the rate-limiting steps of these regimes have been identified through the systematic study of the p_{H2}-dependencies of the hydriding velocity. Next, the effect of a growth-induced internal stress on both the ad- and absorption rate constants has been identified as well. The experimental setup used here has already been presented in detail in a previous publication [20]. A vacuum chamber is first

pumped to a base pressure on the order of 10-6 mbar. Ultra-pure Ar/H_2 gas mixtures (Alphagaz grade from Air Liquide) are then introduced into the chamber to instantaneously impose a desired total pressure, which is continuously measured by two electronic gauges and one back-up manometer. The compositions of the gas mixtures used in this work are 1% and 10%, thereby allowing to further adjust the accessible range of hydrogen partial pressures in the chamber. Although experiments will be reported for p_{H2} values up to 100 mbar, the quantitative stress-affected kinetic analysis - which is the main objective of this study - has been limited to the low p_{H2} range [1 - 10 mbar]. As will be shown below, this allows to avoid the $\alpha \rightarrow \beta$ hydride phase transition. All the experiments presented here have been carried out at room temperature.

A high resolution curvature measurement setup (Multi-Beam Optical Sensor from k-Space Inc.) was mounted onto the hydriding chamber, allowing to continuously detect the positions of multiple laser beams reflecting off a cantilevered sample into a CCD camera. The sample curvature can then be derived from the differential positions of the laser spots [21] as in eq. (1) above. Herein, $\Delta D/Do$ is the mean differential spacing between the reflected laser spots in the CCD, L the distance between the sample and the CCD and α the angle of incidence of the laser beams on the sample. The factor $2L/\cos \alpha$ was calibrated as 1.336 m, based on curvature measurements on mirrors with known radius of curvature. As compared to other curvature or deflection measurement techniques, which are generally based on the position detection of a single reflecting laser beam, our set-up has a significantly improved dynamic curvature resolution on the order of 10 km, thanks to the noise minimization resulting from the use of multiple laser beams. Moreover, thanks to the use of a CCD camera, curvature measurements can be performed with a time resolution better than 100 ms. More details can be found in study A and in [22]. The measured changes in sample curvature, which are a result of the prohibited volume change during Pd-H interaction in the thin film geometry, can be straightforwardly related to a change in internal stress in the Pd layer as in eq. (2) above or in [21], with $Y_S = E_S/(1-v_S)$ the biaxial elastic modulus of the substrate, and t_S and t_f the substrate and Pd film thickness, respectively.

Finally, a direct proportionality can be established between the stress change state and the bulk hydrogen content n in the Pd film, as long as the deformation resulting from these hydriding-induced stresses remains elastic (a condition that will be

explicitly validated below) [23]. This proportionality is given by eq. (3) above, E_f and v_f being, respectively, the Young modulus and Poisson ratio of the Pd film, and n the bulk H/Pd atomic ratio. The ratio between $\Delta V/V$ and n is equal to $\Delta v/\Omega_{Pd}$, where Δv is the characteristic volume change per hydrogen atom and Ω_{Pd} is the mean atomic volume of a Pd atom. Eq. (3) then enables a link between the measured hydriding-induced stress changes $\Delta\sigma$ and the bulk H/Pd atomic ratio n, involving a number of mechano-physical constants, which for convenience are grouped together into a single proportionality factor Q.

The cantilevered samples used for the kinetic analysis were cut approximately 3x0.5 cm^2 in size from oxidized, 380 µm thick Si wafers. These were coated by sputtering with a 170 nm thick Pd thin film, on top of a 5 nm Ti adhesion layer. A high resolution curvature measurement setup, identical to the one described above for the study of the hydriding kinetics of our Pd thin films, has been coupled to the sputtering setup (AJA International, Inc.). As the sputtered films have all been deposited at room temperature in this work (T/T_m = 0.16, where T_m is the Pd melting point [24]), and according to the well-known Thornton diagram [25], the low surface mobility of the atoms at such a deposition temperature does not allow for grain boundary migration or recrystallisation and therefore can be expected to result in the formation of nanocrystalline films with columnar grains. The growth-induced stress in the deposit, which will be used as parameter to study the effect of internal stress on the hydriding kinetics, was varied by changing the argon sputtering pressure (p_{Ar}). It can indeed be expected that the lower the sputtering pressure, the higher the mean free path and therefore also the higher the impact energy of sputtered atoms arriving at the surface of the deposit. This will in turn result in an increased compressive component of the growth stress in the film [26]. This is confirmed in Figure 25, which shows the stress*thickness product as a function of time (before and during Ti layer deposition, as well as after Pd deposition) and Pd thickness (during Pd deposition). An initial baseline curvature measurement was first carried out before Ti deposition at p_{Ar} = 3 mTorr for all samples. Although a detailed interpretation of these growth stress curves is outside the scope of the current paper, we can point out that the stress in the Ti film is slightly tensile during the first stages of deposition, and then becomes compressive after the deposit has turned from isolated aggregates to a continuous layer [27]. The growth-induced stress in the Pd layer is slightly compressive in the first tens of nanometers, and then reaches a constant value given by the constant slope of the

stress*thickness vs. thickness curves. Both the sign and magnitude of the latter is indeed observed to strongly depend on the value of p_{Ar} used during Pd deposition. The resulting mean internal stress values of the as-deposited Pd films, further denoted as σ_0, are given in Table 2, and vary from -152 MPa to 453 MPa for p_{Ar} ranging from 1.5 to 8 mTorr.

Table 2:

Argon plasma pressure p_{Ar}, average growth-induced stress σ_0, thickness t_f, density ρ_f, grain size and (111) texture factor of the Pd films studied in this work.

p_{Ar} [mTorr]	σ_0 [MPa]	t_f [nm]	ρ_f [g/cm³]	grain size [nm]	(111) texture factor [-]
1.5	-152	180	10.4	29	59
3	-55	170	11.0	26	107
4	61	173	10.5	29	93
5	272	160	11.5	27	115
8	453	171	9.8	24	66

The same table 2 also includes results from elementary microstructural characterizations. Cross-sectional and plane-view SEM observations allowed to measure the thickness and grain size of all Pd samples, leading to average values of, respectively, 170 ± 7 and 27 ± 1 nm. Knowing the Pd thin film thickness, Inductively Coupled Plasma (ICP) measurements have been performed on layers dissolved in a $HCl/HNO_3/CH_3COOH$ mixture in order to obtain their density ρ_f. These data indicate an average density for our Pd films of 10.6 ± 0.3 g/cm³, slightly lower than the Pd bulk density of 12 g/cm³ [24]. No trend however is visible in the density data as a function of p_{Ar}. Finally, X-ray diffractograms, using Cu Kα radiation and recorded with an angle step of 0.02°, showed that the Pd films are strongly (111) textured, as can be expected for vacuum deposited fcc metallic thin films [28-30]. The texture factor reported in Table 2 was calculated as the ratio of the intensity parameter $(I_{(111)}/(I_{(200)}+I_{(311)})$ measured on our Pd films with respect to the same quantity based on tabulated intensity values for randomised polycrystalline samples in Ref. [31]. Here again, no trend was visible as a function of p_{Ar}.

In the following, the hydriding cycles derived from our in-situ curvature measurement setup are presented first and analyzed in terms of equilibrium hydrogen uptake. Next, kinetic rate expressions are presented and applied to

analyze in more detail the complete hydriding cycle. Finally, the kinetic model is extended to address the effect of internal stress on the hydriding kinetics, based on activation volume theory.

Figure 26 shows typical hydriding cycles recorded at, respectively, p_{H2} = 1.4 mbar and 1.5 mbar using samples cut out from Pd films initially exhibiting, respectively, a 61 MPa and 272 MPa tensile internal stress. As the Pd thin film sample is attached to a substrate, its volume expansion is constrained upon hydriding, leading to the generation of an increasing amount of compressive hydriding-induced stress. This stress then levels off when equilibrium is reached between gaseous hydrogen in the chamber and atomic hydrogen in the film. The initial stage of a hydriding cycle is also shown for a sample initially at -55 MPa, to already show the dramatic slowing down of the hydriding kinetics that occurs when using Pd thin films initially in compression.

In order to proceed with the equilibrium analysis of such hydriding cycles, the explicit assumption underlying eq. (3) of elastic deformation in the Pd film must first be addressed. Besides the hydriding-induced compressive stress change, also the initial, growth-induced stress state of the Pd thin films needs to be considered. As to the latter, Table 2 indicated already that our Pd films show growth-induced stress levels ranging from -152 to 453 MPa. The latter value is above the theoretical tensile yield stress of bulk Pd measured by Sanders et al. [32], but below the yield stress of 550 MPa that they reported for nanocrystalline Pd samples. As to the hydriding-induced stresses, Figure 27 shows room temperature pressure-stress isotherms, obtained by successively increasing the hydrogen partial pressure p_{H2} in the chamber and waiting for equilibrium. It is observed that all the samples end up at about -950 MPa in compression for p_{H2} = 100 mbar, regardless of their initial growth-induced stress state. This observation is in agreement with the measurements of Youngdahl et al. [33], who reported that the compressive yield stress of nanocrystalline Pd is on the order of 1 GPa. In other words, when this yield stress level is reached in our Pd thin films, the direct proportionality between internal stress and hydrogen content as given by eq. (3) vanishes, and the films may still absorb hydrogen without giving rise to a curvature or stress change. Moreover, on the same Fig. 27, the $\alpha \rightarrow \beta$ phase transition can be identified to start at room temperature between 10 and 20 mbar for the film initially at 435 MPa in tension and between 30 and 40 mbar for the film initially at 272 MPa in tension. The

films initially in compression do not exhibit any phase transition between 1 and 100 mbar, while the $\alpha \rightarrow \beta$ phase transition for the film initially at 61 MPa is interrupted when the absolute stress reaches -950 MPa. This shift of the $\alpha \rightarrow \beta$ phase transition lower limit towards higher values of p_{H2} when the initial stress state in the metal increases in the compressive direction, has already been observed for Fe-Pd [6] and Mg [7] compounds. In order to avoid such complicating plasticity and phase transition effects, the present kinetic analysis has therefore been limited to the p_{H2} interval [1 - 10 mbar]. In this range, the equilibrium absolute stress does not exceed -700 MPa for any of our samples, staying well below the compressive yield stress for nanocrystalline Pd thin films [33]. Under these conditions, the proportionality between the hydriding-induced stress change and the bulk hydrogen content n, as given by eq. (3), will remain valid throughout this study.

Based on the above considerations, it is now possible to calculate Sievert's constant K_s in the α-PdH region from the data of Fig. 27, based on Sievert's law $K_s = (p_{H2})^{1/2}/n_{eq}$ [12]. The subscript "eq" refers here to the equilibrium H-uptake, so that n_{eq} can be derived directly from Fig. 27 using Eq. (3). The resulting K_s values, obtained with $\Delta v/\Omega_{Pd} = 0.19$ [34], $E_{Pd} = 121$ GPa and $v_{Pd} = 0.39$ [24], are listed in Table 3. The latter don't show any trend as a function of the initial, growth-induced stress state of the Pd films before hydriding, except for the higher K_s value observed for the sample with the most compressive growth stress. We can already point out here that this sample will not be further considered for the kinetic analysis, as its hydriding behaviour is excessively slow (cfr. Fig. 26). Since K_s has been reported to be a function of the concentration of structural defects in the host metal lattice [35], the data in Table 3 indicate that, while obtaining different growth-induced stress levels in the Pd films by changing the Ar sputtering pressure, one may still arrive to keep the for hydriding most relevant microstructural parameters constant. The same statement was already inferred from the similar elementary characterisation results reported for the different samples in Table 2.

Table 3:

Sievert's constant of the Pd films studied in this work, calculated from the data of Fig. 27 in the α-PdH region.

σ_0 [MPa]	K_s [$^{atm1/2}$]
-152	4.79±0.18
-55	3.53±0.15
61	3.74±0.22
272	3.19±0.12
453	3.94±0.12

Coming back once more to the raw data in Fig. 26, when the equilibrium compressive stress is reached in the sample, the gas mixture is pumped out of the chamber. As a result, the hydriding-induced compressive stress gradually decreases, until a second plateau is reached. This is believed to reflect the presence of residual hydrogen in the thin film under the new low vacuum conditions. For all the hydriding cycles presented here, this residual compressive stress change, i.e. the difference between the absolute stress at the beginning and at the end of the hydriding cycle, is on the order of 200 MPa. It has already been shown before to disappear upon venting [23], and therefore cannot be attributed to a plasticity effect.

Before, we already presented a kinetic model able to provide a self-consistent interpretation of the entire room temperature hydriding cycle of Pd thin films in the α-phase domain [23]. Its constitutive equations have been derived starting from the observation that two mechanistic steps are potentially rate-limiting during Pd thin film hydriding. One of them includes H_2 adsorption and its dissociative chemisorption on the Pd surface. The second one is absorption and involves an equilibrium reaction between atomic hydrogen at, respectively, surface and interstitial bulk sites. These two steps can be written as in eqs. (5) and (6). No diffusion step is taken into account in this model because of the very small room-temperature diffusion time on the order of milliseconds in the case of Pd films that are only 170 nm thin [23]. The derivation of rate expressions corresponding to the ad- and absorption limited regime has been carried out by assuming a specific rate-controlling step, and by considering the other one to be in a pseudo steady-state. This method is the common way to proceed in chemical kinetics when dealing with

complex second order reactions [36]. The time evolution dn/dt of the bulk H/Pd atomic ratio when the rate-limiting step is, respectively, adsorption and absorption have thus been shown to take on the form of eqs. (19) and (18) [23]. In these equations, $K_{ad} \equiv k'_{ad}/k''_{ad}$ and $K_{ab} \equiv k'_{ab}/k''_{ab}$ are, respectively, the equilibrium constants of reactions (5) and (6).

The hydriding cycles in Fig. 26 for the samples with an initial tensile growth-induced internal stress exhibit three characteristic kinetic regimes. At the beginning, a first linear region is observed in the stress-time curves. This has been shown before to correspond to an absorption-limited kinetic regime, adsorption still being relatively unconstrained on the freshly exposed Pd surface. A transition to a second linear kinetic regime is then observed, which we have already attributed before to a change of the heat of adsorption in the positive direction as the surface coverage reaches a critical value [37]. As a result of the associated decrease in stability of the adsorbed hydrogen atoms, adsorption then becomes the new rate-limiting step in this second kinetic regime. The amount of hydrogen in the sample continues to increase linearly with time until adsorption equilibrium is reached. This marks the end of the second linear kinetic regime. Absorption then becomes rate-limiting again and a third, nonlinear kinetic regime is observed until absorption equilibrium is reached ($n = n_{eq}$).

The slopes of the first and second linear kinetic regimes have been plotted as a function of p_{H2} in, respectively, Figures 28 and 29. Since the time scale involved in the hydriding of samples initially under compression was excessively large (cfr. Fig. 26), our kinetic analysis has been limited to samples with an initial tensile growth-induced stress, as already mentioned before. In Fig. 28, the effect of the initial internal stress state of the Pd films is clearly visible. This indicates that at least one of the parameters of the absorption-limited rate equation Eq. (18) is affected by internal stress. Since K_s was shown before in Table 3 to be stress-independent in the σ_0–range considered here, the stress-affected kinetic parameter in Eq. (18) should be k'_{ab}. As was already inferred from Fig. 26, increasing the internal stress in the tensile direction leads to a faster rate of hydrogen uptake in the first, absorption-limited kinetic regime. From the results in Figure 29, it is seen that this is not the case in the second, adsorption-limited regime. Indeed, no statistical differences could be observed between data points coming from the three batches, leading to one single linear fit. As a result, the parameters of the adsorption-limited rate equation (19) can be considered to be independent of the internal stress state

of the film. The observed linear p_{H2} dependence as such observed in both Figure 28 and 29 will be justified below. The above observations agree with intuition, in that the stress due to hydrogen uptake by the Pd films is compressive, so that one may expect an additional driving force for hydriding when stretching the host lattice in the tensile direction. At the free surface however, no significant volume expansion occurs during adsorption, making the latter much less sensitive to internal stress effects inside the film.

We now proceed with a quantitative analysis of the absorption rate constant k'_{ab}. For this purpose, the temporal evolution of n for an absorption-limited kinetic regime has first been deduced by integrating Eq. (18), which is known as a basic Cauchy problem and results in a solution according to eq. (30) with constants as specified in eq. (29) [38]. The fitting constant C_2 thereby gives direct access to the parameter of interest k'_{ab}. Figure 30 shows the thus obtained values of k'_{ab} in the first kinetic regime for the same experiments already presented in Fig. 28. As expected from the data in Fig. 28, k'_{ab} increases for a given p_{H2} when increasing the growth-induced internal stress in the tensile direction. Besides being stress-affected, k'_{ab} also turns out to exhibit a linear dependence with p_{H2}. In their hydrogen membrane permeation model [39], Ward et al. suggested that k'_{ab} may indeed depend on surface coverage at freshly exposed surfaces, which is the case in the first kinetic regime.

The dependence of k'_{ab} on both internal stress and p_{H2}, as unraveled in Fig. 30, can be quantified as follows. Firstly, based on the general expression for the hydrogen absorption rate constant k'_{ab} [39-41]

$$k'_{ab} = A_{ab}.\exp\left[\frac{-\Delta H_{ab}^{0_+^+}}{RT}\right] \qquad (31)$$

where $\Delta H_{ab}^{0_+^+}$ represents the standard activation enthalpy change related to hydrogen absorption, its linear p_{H2}-dependence unraveled in Fig. 30 can simply be taken into account by writing the pre-exponential factor for hydrogen absorption A_{ab} as a product $A'_{ab}.p_{H2}$

$$k'_{ab} = A'_{ab}.p_{H_2}.\exp\left[\frac{-\Delta H_{ab}^{0_+^+}}{RT}\right] \qquad (32)$$

We can now also justify the observed linear p_{H2} dependence of the data in Fig. 28. The latter are proportional to the hydrogen absorption rate $(dn/dt)_{ab}$ given by eq. (18), where the parameter k'_{ab} is now known to include an additional linear p_{H2} dependence.

Moreover, the last term can be shown to vanish when n << 1, as is indeed the case for the initial stages of hydriding in the p_{H2}-range 1-10 mbar corresponding to the α-PdH phase considered here.

With respect to the stress-dependence, according to the schematic energy diagram for hydrogen ad- and absorption, reproduced from ref. [39] in Figure 31, the standard activation enthalpy change $\Delta H_{ab}^{0_+^+}$ in the absence of an internal stress field is equal to the activation energy E_a needed for a hydrogen surface-to-bulk transition. In order to take into account that the host lattice undergoes a biaxial stress σ, the standard activation enthalpy change of absorption can be written as [42] :

$$\Delta H_{ab}^{0_+^+} = E_a - \frac{2V\sigma}{3} \tag{33}$$

where V represents the activation volume for hydrogen absorption, and 2σ/3 is the hydrostatic stress on the Pd crystalline lattice. Hence, the presence of internal stress will decrease the energy barrier for H-absorption, thereby increasing the rate constant k'_{ab}. The representative activation volume V for hydrogen absorption can be extracted by combining Eqs. (32) and (33):

$$\frac{\partial \ln\left(k'_{ab} / p_{H_2}\right)}{\partial \sigma} = \frac{2V}{3RT} \tag{34}$$

In Fig. 32, the slopes of the k'_{ab} curves corresponding to the samples presented in Fig. 30 have been plotted as a function of the growth-induced internal stress in the Pd thin films. The slope of the linear fit in this graph leads to an activation volume V = 17.6 ± 2.3 Å³ for H-absorption into our Pd thin films. This value, for which to the best of our knowledge no other experimental literature data exist, is high with respect to the value of 2.0 ± 0.3 Å³ obtained by Baranowski and Majorowski for the activation volume for hydrogen diffusion in palladium hydride [43]. This observation seems meaningful because in the case of diffusion, the hydrogen atoms jump between equivalent bulk interstitials sites. In the case of H-absorption, the hydrogen atoms jump from Pd surface sites, where the lattice is highly distorted, to bulk interstitial sites, where the hydrogen concentration is much smaller and the lattice is much less distorted [44]. This mechanism may therefore require a much higher activation volume. Our measured activation volume for H-absorption, combined with an internal tensile stress on the order of 450 MPa in our nanocrystalline Pd films, leads to a decrease of the activation energy E_a for H-

absorption of 3 kJ/mol. This decrease may seem small with respect to typical values for $E_a \cong 66$ kJ/mol [39] reported in the literature. However, its effect is not all negligible, leading to a factor 3.3 increase in the room-temperature absorption rate in the initial stages of hydriding corresponding to the first kinetic regime. Therefore, it may lead to interesting applications, increasing for instance the response time of integrated hydrogen sensors, or allowing to decrease the temperature of charging/discharging in storage applications.

With respect to the data of the second, adsorption-limited kinetic regime, the rate constant for hydrogen adsorption k'_{ad} has been calculated as well, based on Eq. (19) and using a 4th order Runge-Kutta algorithm to simulate the temporal evolution of n. As expected from the data already presented in Fig. 29, the fitted k'_{ad} values do not show any trend as a function of the growth-induced internal stress. Their mean values, averaged over the experimentally-covered p_{H2} range 1-10 mbar, are, respectively,

$(1.1 \pm 0.1) \times 10^{21}$ [mbar^{-1}s^{-1}] for $\sigma_0 = 61$ MPa,

$(1.0 \pm 0.2) \times 10^{21}$ [mbar^{-1}s^{-1}] for $\sigma_0 = 272$ MPa and

$(1.3 \pm 0.2) \times 10^{21}$ [mbar^{-1}s^{-1}] for $\sigma_0 = 453$ MPa.

The absence of any p_{H2}-dependence for k'_{ad} can be expected from the basic expression of its pre-exponential factor [37,39]. The latter can indeed be written as $1/(2\pi m_{H2} k_B T)^{1/2}$, where m_{H2} is the molecular mass of H_2 and k_B is the Boltzmann constant. This also allows to justify the linear fit used in Fig. 29, confirming the linear p_{H2}-dependence of $(dn/dt)_{ad}$ predicted in eq. (19).

Finally, the rate constant for hydrogen absorption k'_{ab} has been calculated as well in the third kinetic regime, using the same algorithm as in the first regime. Figure 33 shows the evolution of the bulk hydrogen concentration in this case, as calculated at different p_{H2}-values from the internal stress data for the batch of samples initially at $\sigma_0 = 61$ MPa. The time scale was normalised to represent for each experiment the first 40s of the third kinetic regime. Excellent agreement is obtained in all cases with the constitutive eq. (30), confirming that the third kinetic regime is indeed limited by absorption. The mean k'_{ab} values for the three batches of samples, averaged over the experimentally-covered p_{H2} range 1-10 mbar, are, respectively,

$(3.6 \pm 0.8) \times 10^{-3}$ [s^{-1}] for $\sigma_0 = 61$ MPa,

$(3.4 \pm 0.8) \times 10^{-3}$ [s^{-1}] for $\sigma_0 = 272$ MPa and

$(3.9 \pm 0.9) \times 10^{-3}$ [s^{-1}] for $\sigma_0 = 453$ MPa.

Contrary to the k'_{ab} values obtained in the first kinetic regime, no trend is visible in this case, neither as a function of the initial, growth-induced internal stress, nor as a

function of p_{H2}. As to the independence with p_{H2}, this can be understood as follows: while k'_{ab} may depend on the surface coverage and thus on p_{H2} at low surface coverage [39], this cannot be the case anymore when the surface coverage is at equilibrium, as is the case in the third kinetic regime. The independence with internal stress might at first seem more surprising, in view of the results obtained for the first kinetic regime which was also absorption-limited. However, some important differences exist with respect to the hydriding state of the Pd films in the first and the third regimes. First of all, the absolute stress in the films in the third regime is a compressive one (cfr. Fig. 26). Our results therefore seem to indicate that any stress-affect on the absorption kinetics might only become significant for samples under tension. Secondly, in the third regime, samples are close to the equilibrium state of hydrogen uptake ($n \cong n_{eq}$). This may suggest that the absorption rate only becomes stress-modulated in a sample volume that is still relatively free of hydrogen. Finally, the values of k'_{ab} calculated for the third kinetic regime are roughly one order of magnitude higher than those of the first kinetic regime. This is in agreement with our earlier observations [23], and was attributed to a change of the heat of adsorption of about 6 kJ/mol when the surface coverage reaches a critical value at the end of the first kinetic regime. This change being twice as much as the stress-affected change in activation energy, the kinetics of hydrogen absorption in the third kinetic regime can therefore be expected to be mainly driven by an increased surface repulsion of dissociatively chemisorbed hydrogen.

A high resolution in-situ curvature measurement set-up has been used in this study to study the effect of pre-existing growth-induced internal stress on the hydriding kinetics of nanocrystalline Pd thin films. Three kinetic regimes have been resolved. The first kinetic regime has been found to be limited by absorption, and the second one by adsorption. A switch back to absorption-limited kinetics is finally observed before the final equilibrium. The analysis of the effect of internal stress on the absorption kinetics in the first kinetic regime shows that tensile stresses accelerate the hydriding kinetics, while compressive stresses dramatically slow down the hydriding kinetics. No effect of internal stress on the adsorption kinetics has been observed. A quantitative analysis of the p_{H2}- and internal stress dependence of the rate constant of the first kinetic regime enabled to calculate the activation volume for hydrogen absorption into our nanocrystalline Pd thin films.

It is supposed that the present invention is not restricted to any form of realization described previously and that some modifications can be added to the presented example of fabrication without reappraisal of the appended claims. For example, the present invention has been described referring to a Pd thin film, but it is clear that the invention can be applied to a Mg thin film for instance or to a metallic alloy or a ceramic.

CLAIMS

1. A device for the improved uptake, storage and release of hydrogen, comprising:
   - a solid-state active element capable of taking up, storing and releasing hydrogen; and
   - stress-inducing means attached to the active element,

   characterized in that

   said stress-inducing means are capable of applying a mechanical load to the active element.

2. A device according to claim 1, whereby said stress-inducing means comprise an electromechanical device attached to at least one side of the active element, said electromechanical device capable of pushing and pulling at said side of said active element thereby capable of inducing compressive or tensile stress in the active element, said electromechanical device controlled by an electrical control circuit.

3. A device according to any of claim 1 or 2, whereby said solid-state active element comprises a thin-film on a substrate.

4. A device according to claim 3, whereby said active element is mounted on a fixed frame at or near the in-plane sides of said active element and said stress-inducing means comprise at least one piezo-electric crystal located at or near the middle of said active element and capable of pushing or pulling at said substrate and said thin film of said active element, thereby capable of bending said active element out of its plane.

5. A device according to any of claims 3 or 4, whereby said stress-inducing means comprise a lattice mismatch between said thin film and said substrate of said active element and/or any other microstructural or thermal origin leading to internal stress inside the thin film.

6. A system for the improved uptake, storage and release of hydrogen, comprising:
   - one or more devices according to any of claims 1 to 5; and
   - an air-tight container in which said devices are mounted,

   characterized in that

   said air-tight container comprises one or more in- and/or outlets for H_2-gas and one or more control mechanisms for the stress-inducing means of said one or more devices.

7. A method for the improved uptake of hydrogen in a device according to any of claims 1 to 5, comprising the steps of:
   - applying a mechanical load to said active element of said device by said stress-inducing means; and
   - bringing the surface of said active element into contact with H_2-gas under a predetermined temperature and pressure.

8. A method for the improved storage of hydrogen in a device according to any of claims 1 to 5, comprising the steps of:
   - applying a mechanical load to said active element of said device by said stress-inducing means;

9. A method for the improved release of hydrogen in a device according to any of claims 1 to 5, comprising the steps of:
   - applying a mechanical load to said active element of said device by said stress-inducing means; and
   - evacuating the H_2-gas which is released by said active element.

10. A method for providing a fuel cell with hydrogen gas, comprising the steps of:
   - loading the active elements of a system according to claim 6, by means of a method according to claim 7, whereby the H_2-gas is provided via said in- or outlets of said system;
   - storing hydrogen in the active elements of said system by means of a method according to claim 8; and
   - releasing hydrogen from the active elements by means of a method according to claim 9 whereby the released H_2-gas is evacuated via said in- or outlets of said system and provided to said fuel cell;

FIGURES

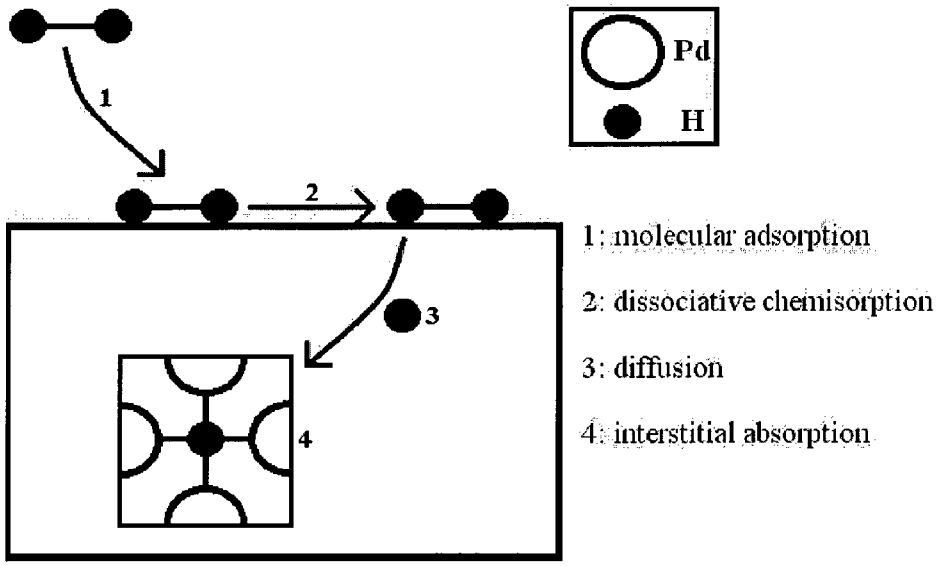

Figure 1a

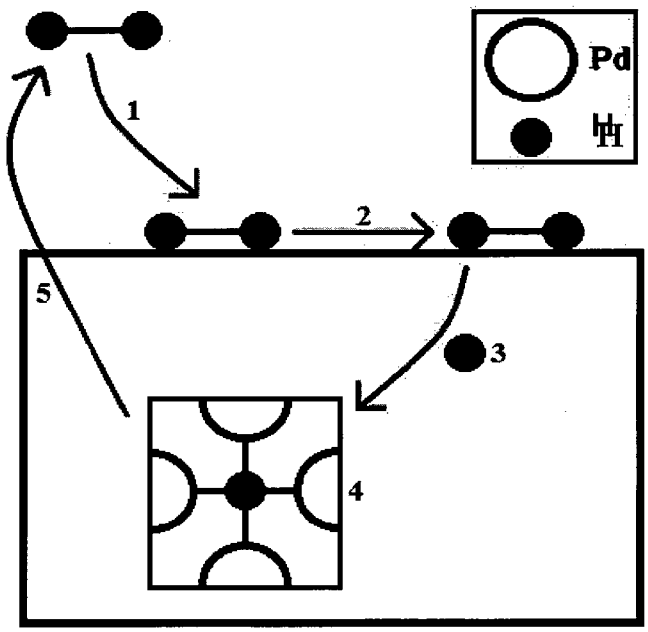

Figure 1b

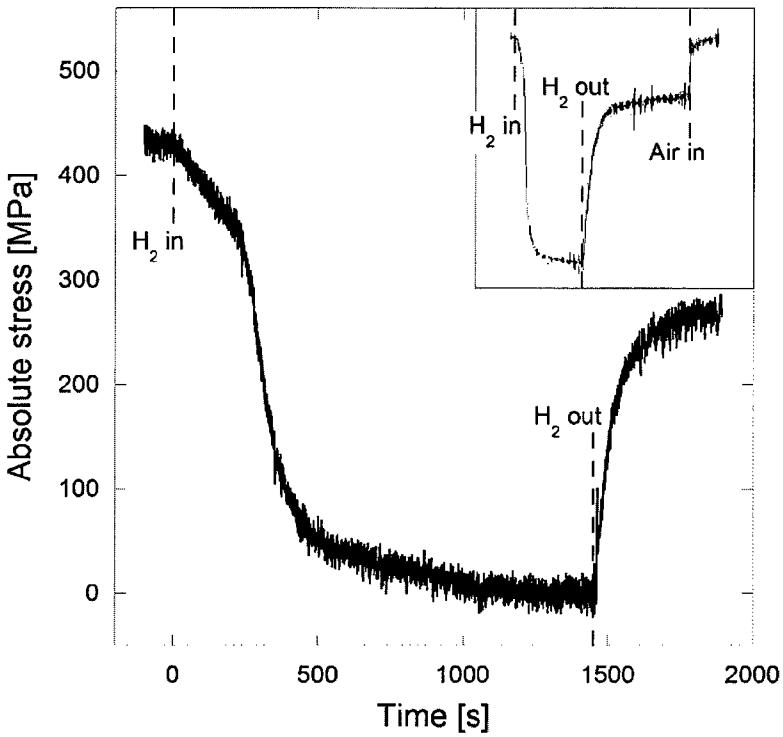

Figure 2a

Venting after vacuum dehydriding

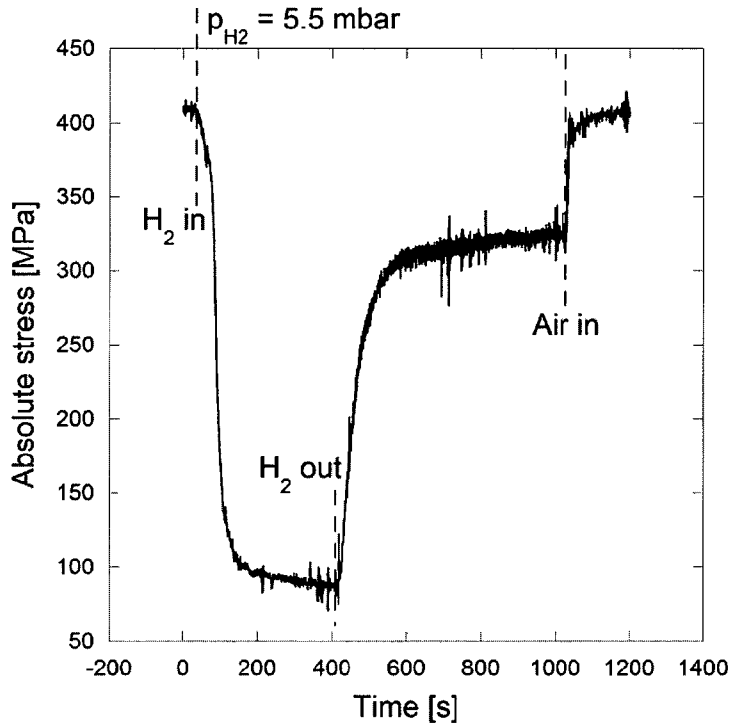

Figure 2b

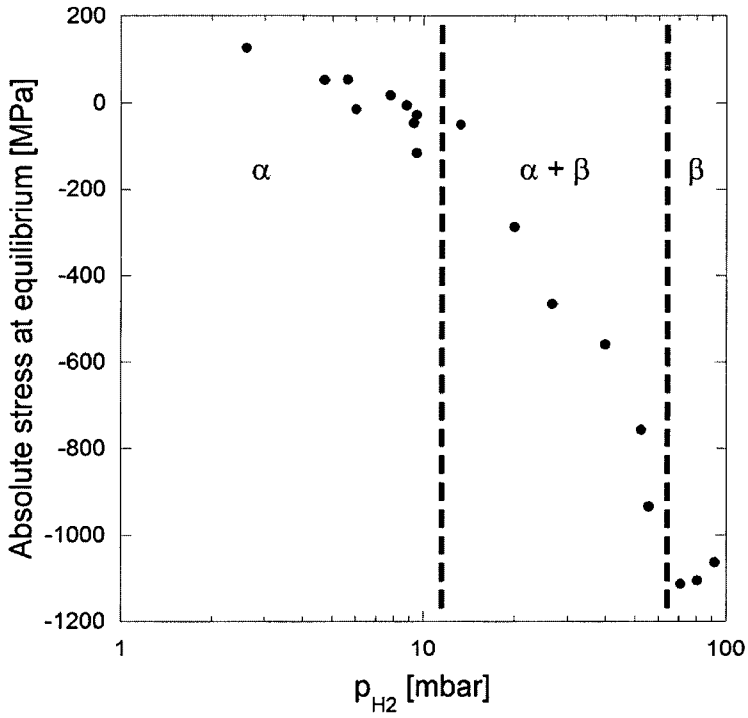

Figure 3

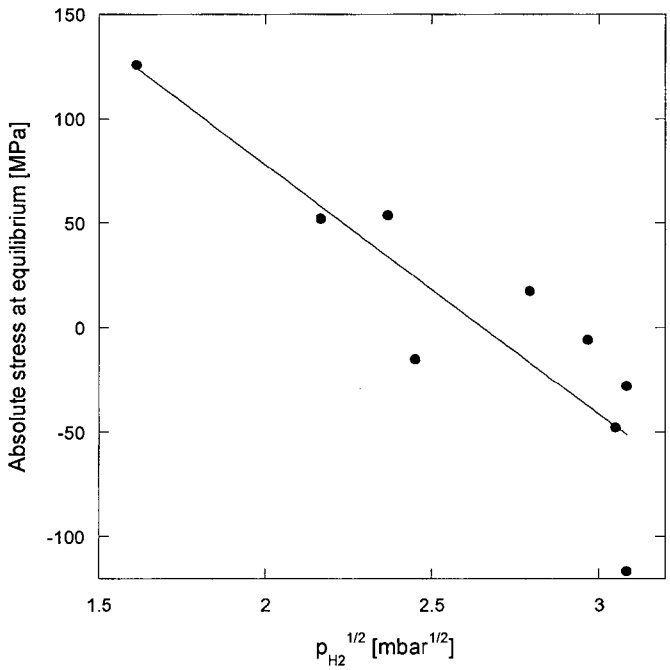

Figure 4

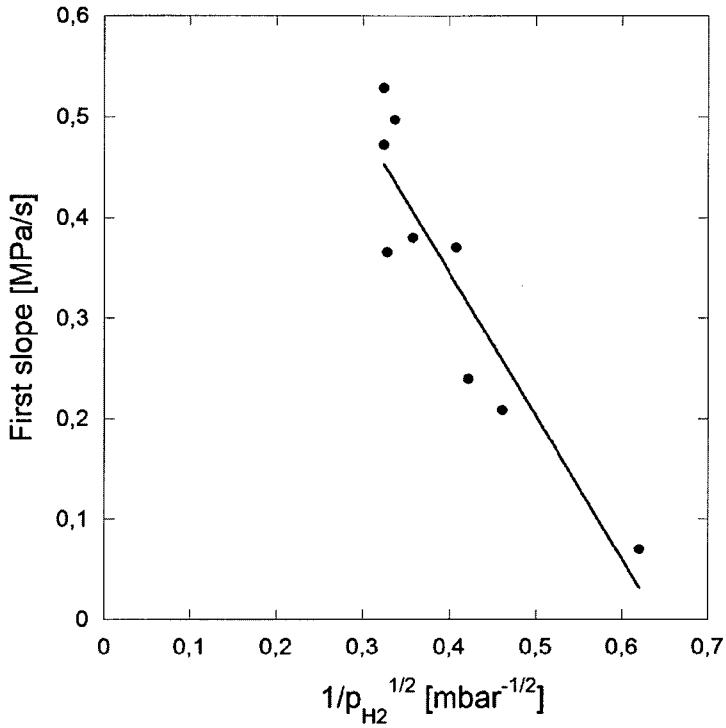

Figure 5a

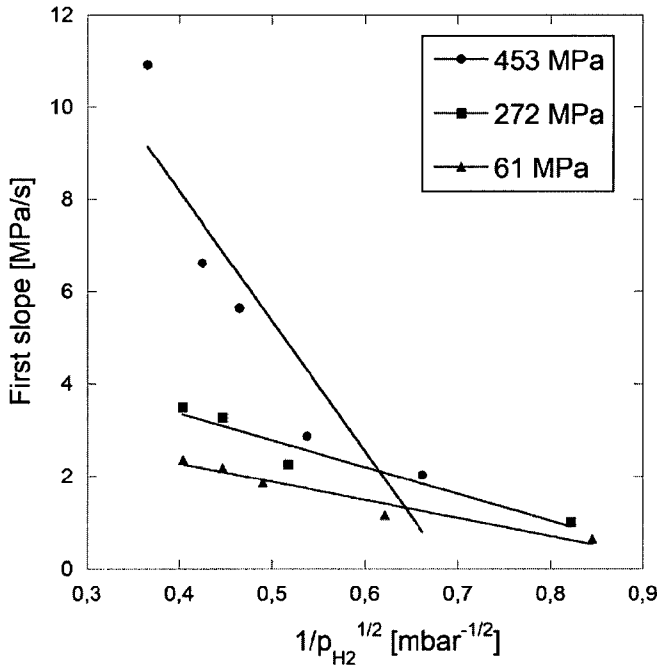

Clear effect on 1st kinetic regime
→Absorption kinetics affected

Figure 5b

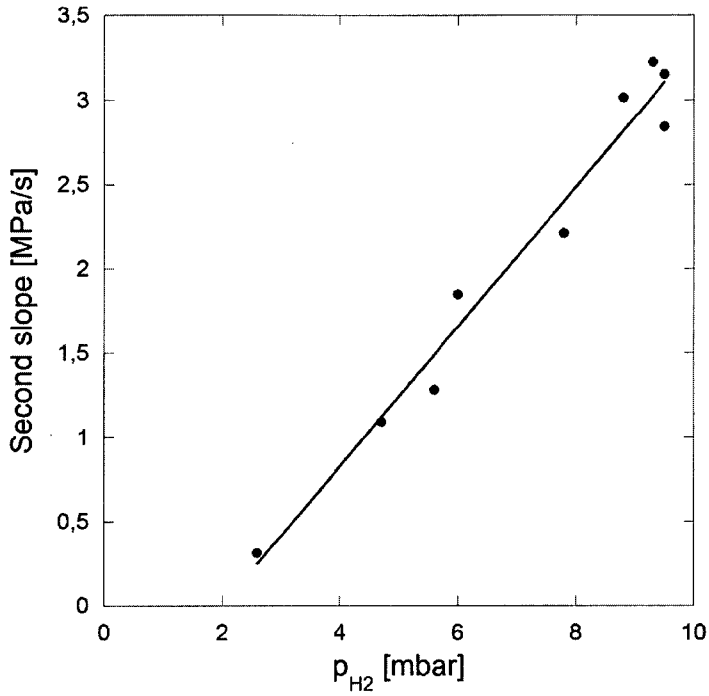

Figure 6a

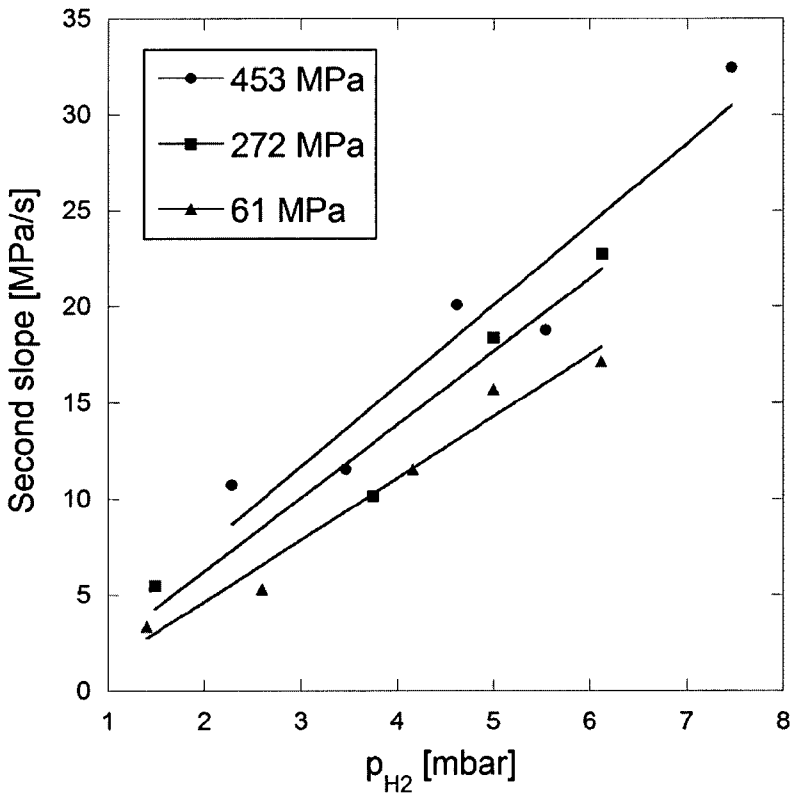

No clear effect on 2nd kinetic regime
→Adsorption kinetics unaffected

Figure 6b

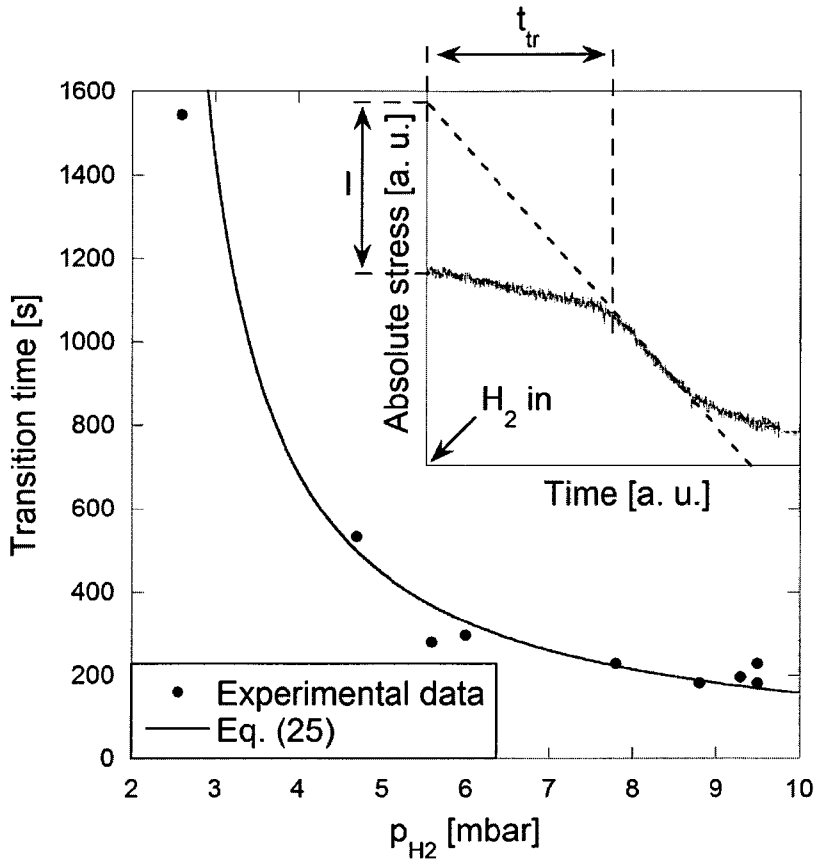

Figure 7

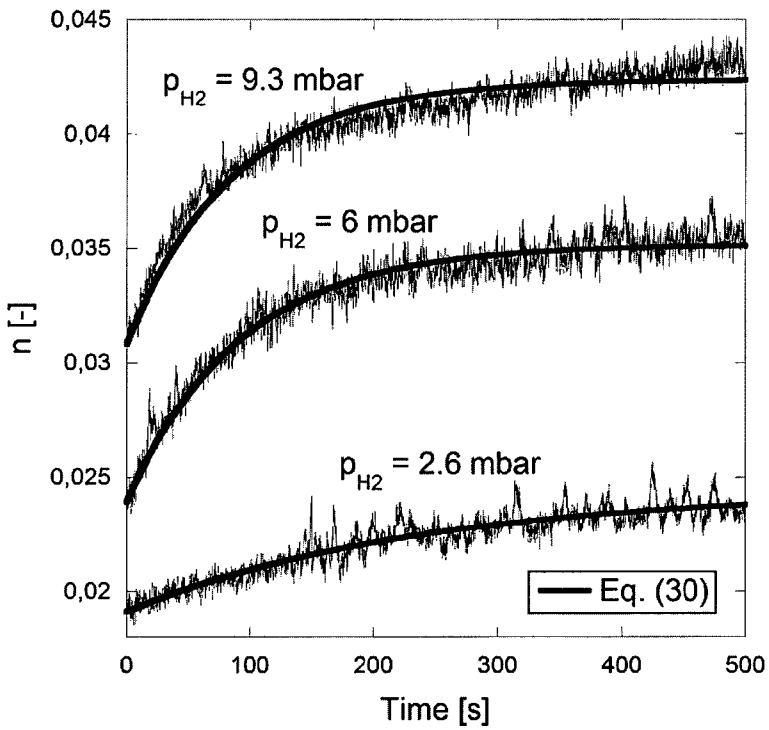

Figure 8

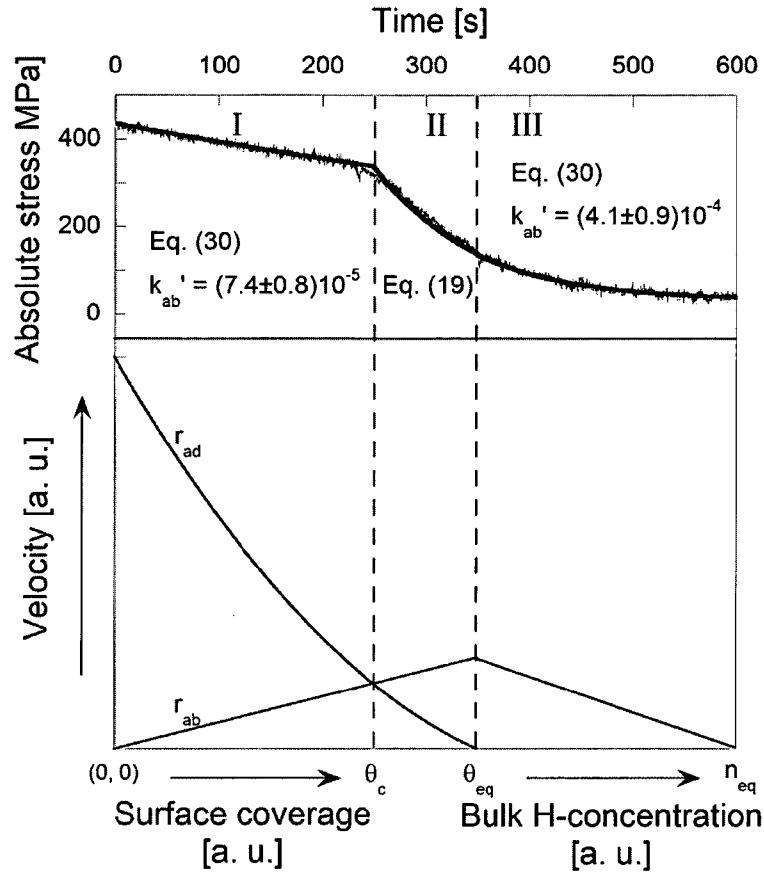

Figure 9

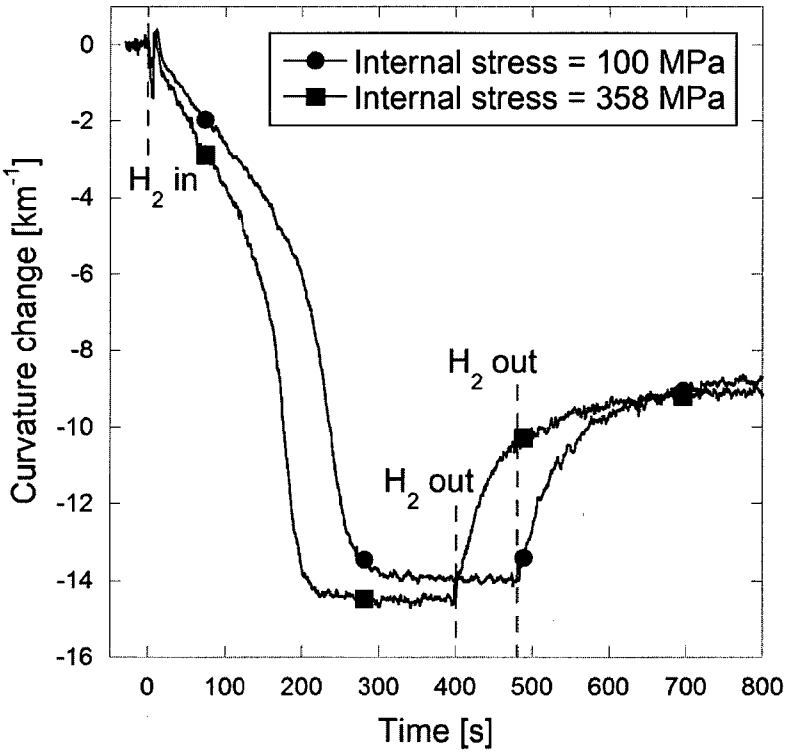

Figure 10a

Internal stress effect:
- Tensile stresses accelerate kinetics
- Compressive stresses dramatically slow down kinetics

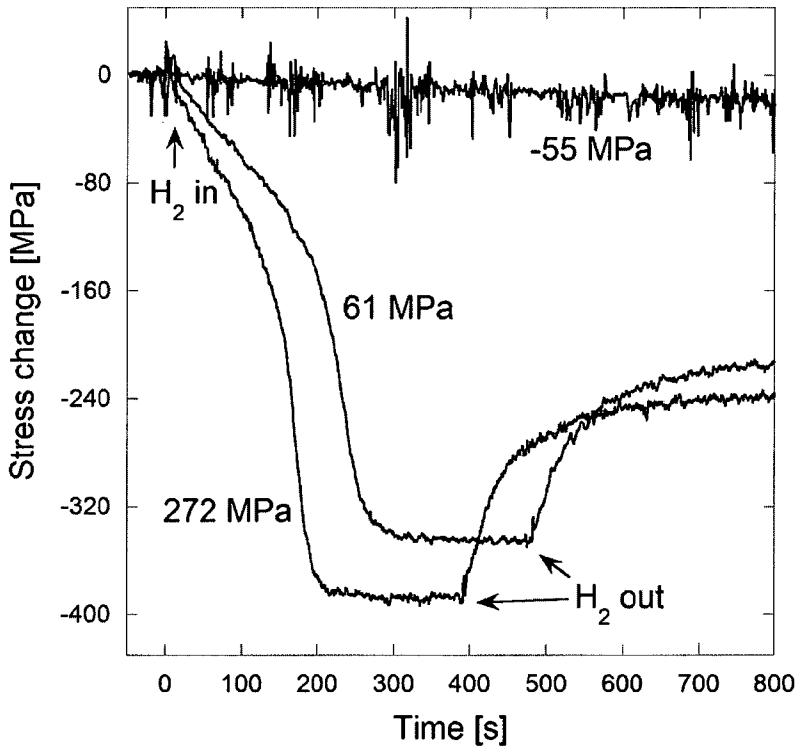

Figure 10b

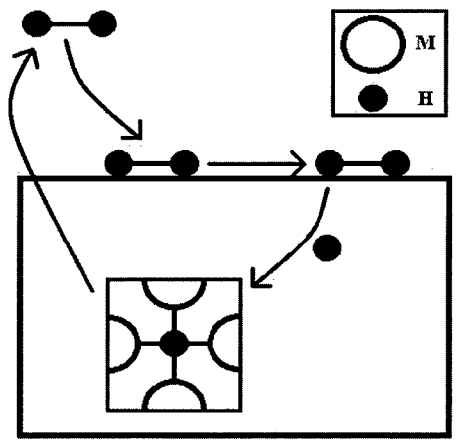

Figure 11

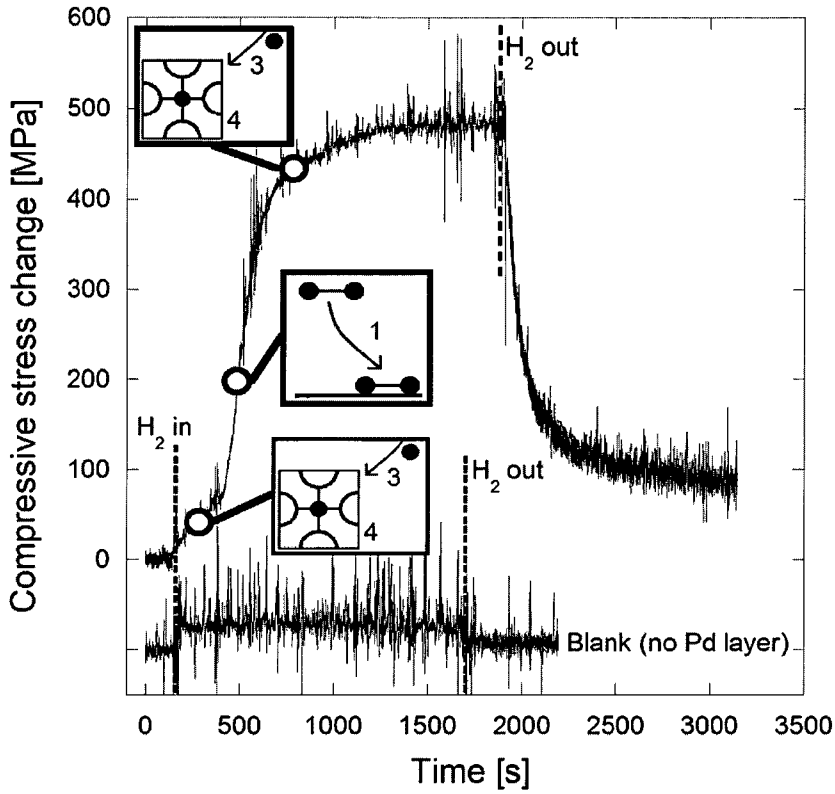

Figure 12

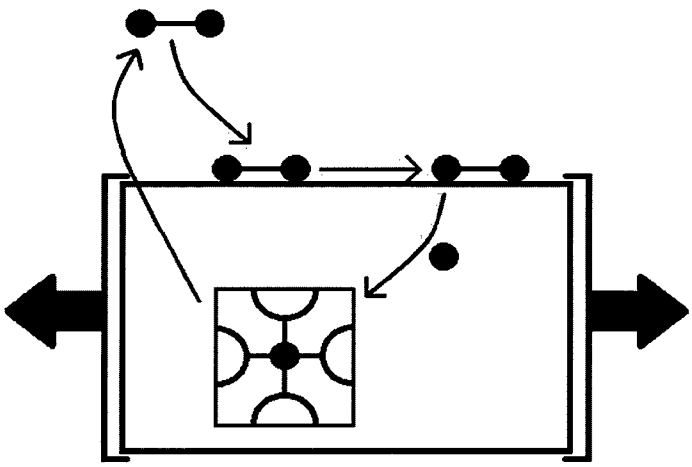

Figure 13

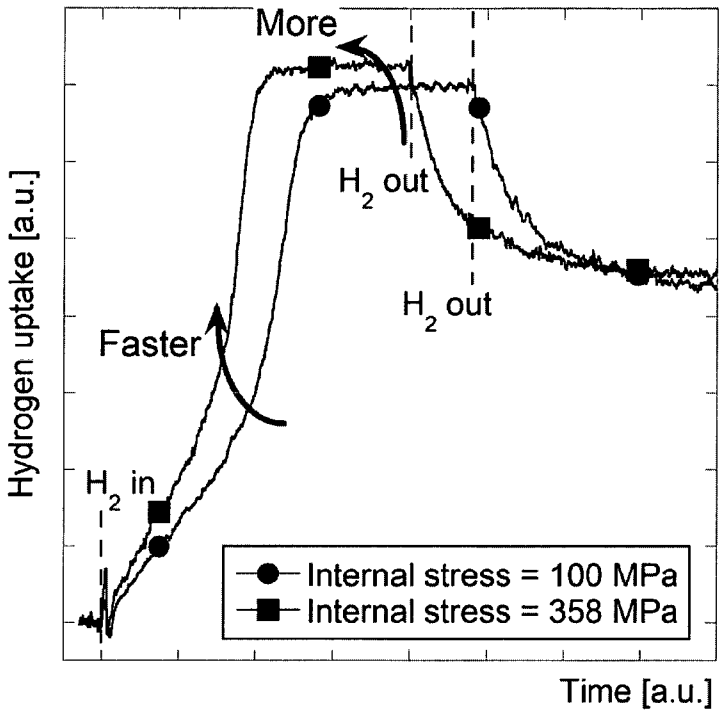

Figure 14

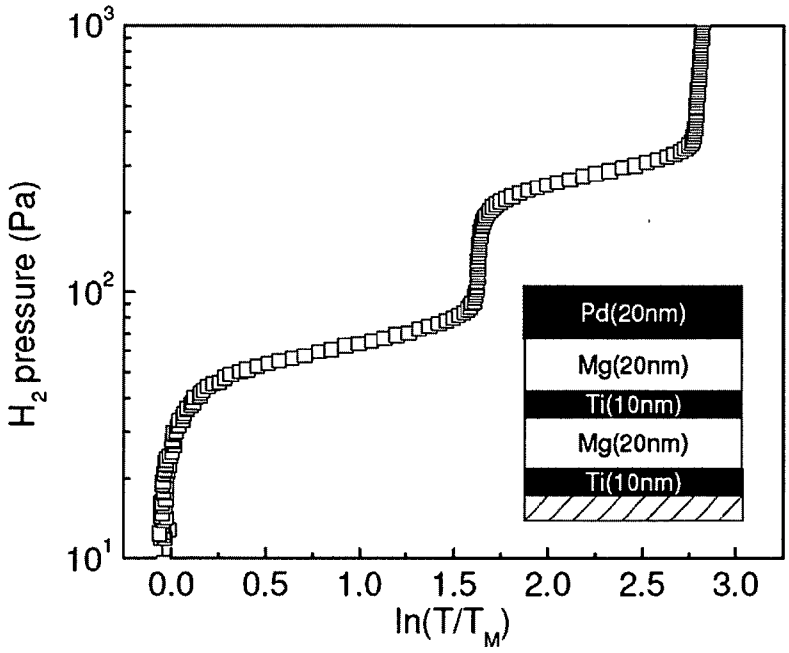

Figure 15

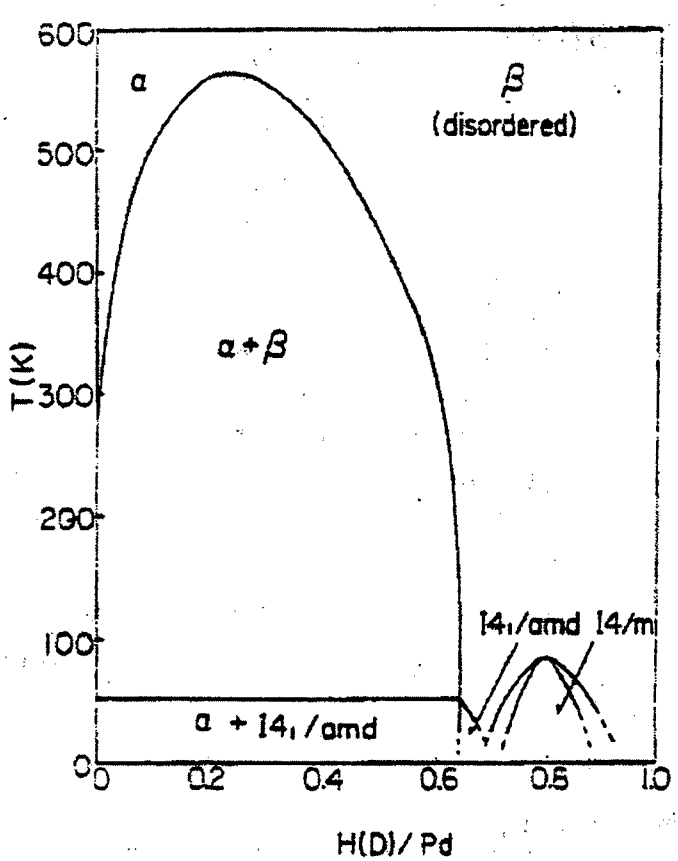

Figure 16

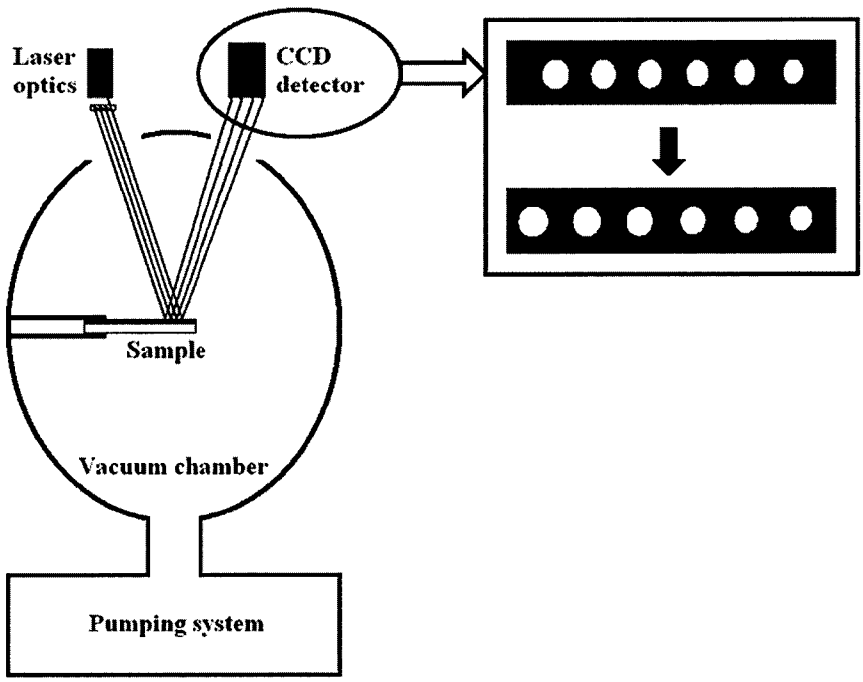

Figure 17

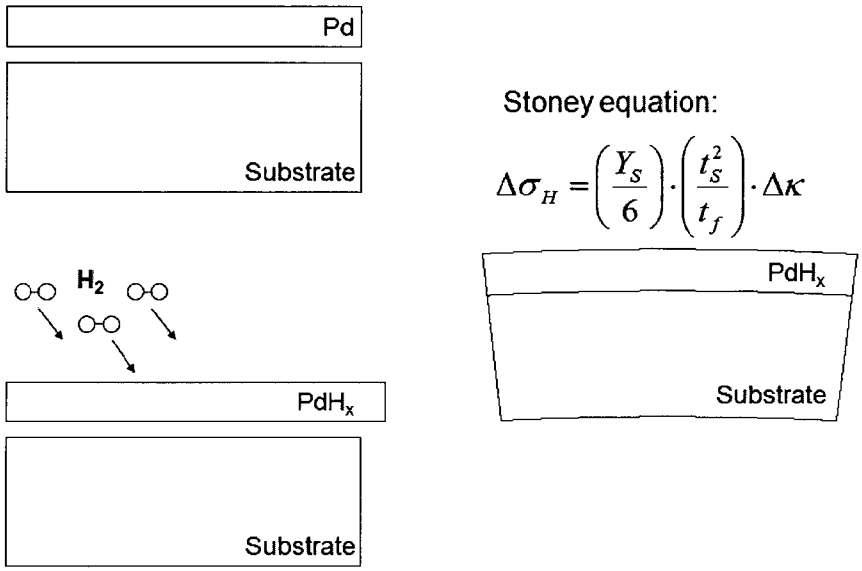

Figure 18

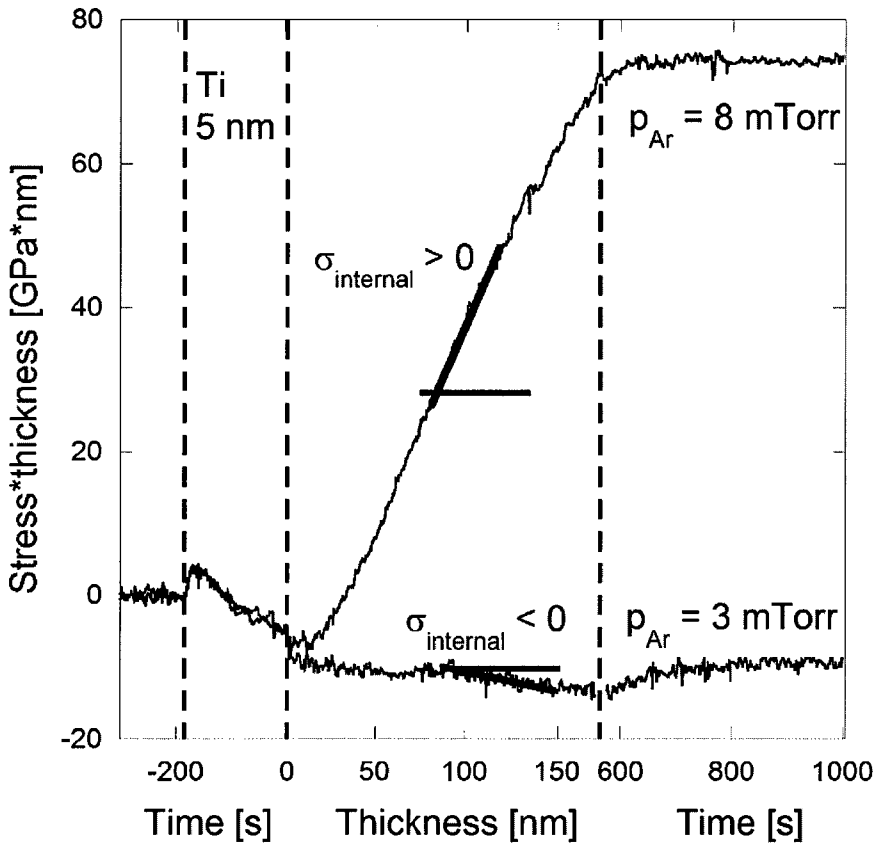

Figure 19

Thin film characterization

Internal stress [MPa]	Pd thickness (SEM) [nm]	Density (ICP) [g/cm³]	Grain size (SEM) [nm]	(111) texture factor [-]
-152	180	10.4	29	59
-55	170	11	26	107
61	173	10.5	29	93
272	160	11.5	27	115
453	171	9.8	24	66

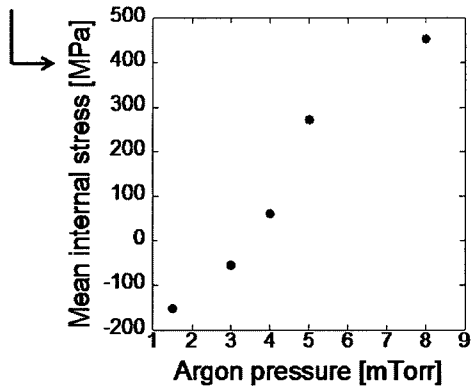

Mean density: 10.6 ± 0.3 g/cm³

Mean grain size: 27 ± 1 nm

Mean texture factor: 88 ± 11

Figure 20

Evolution of the heat of adsorption

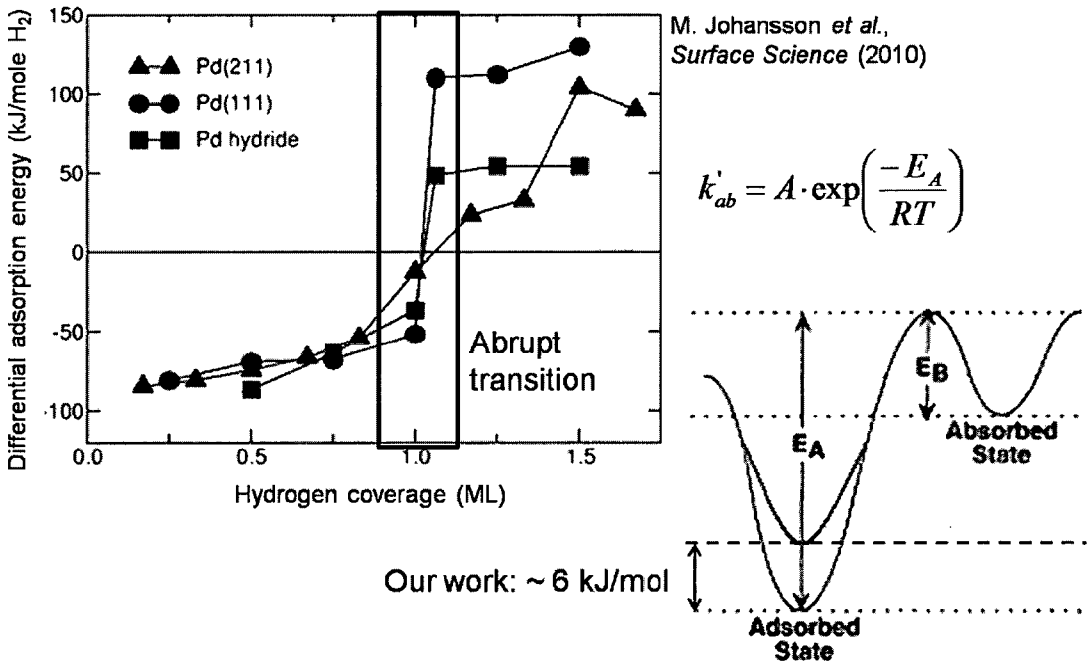

Figure 21

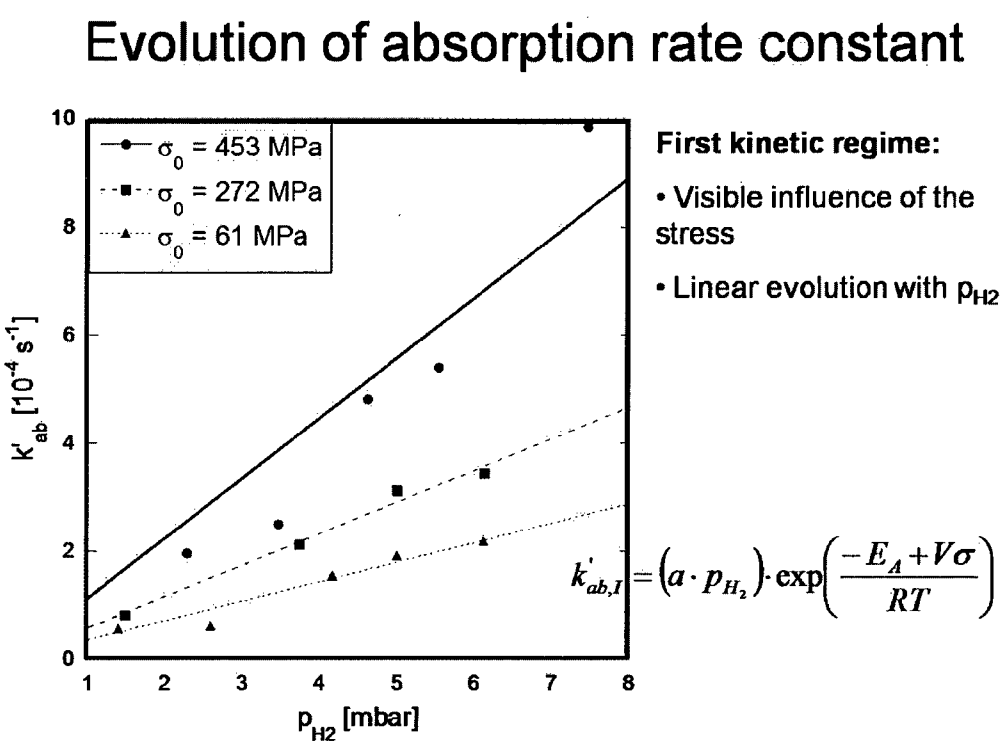

Figure 22

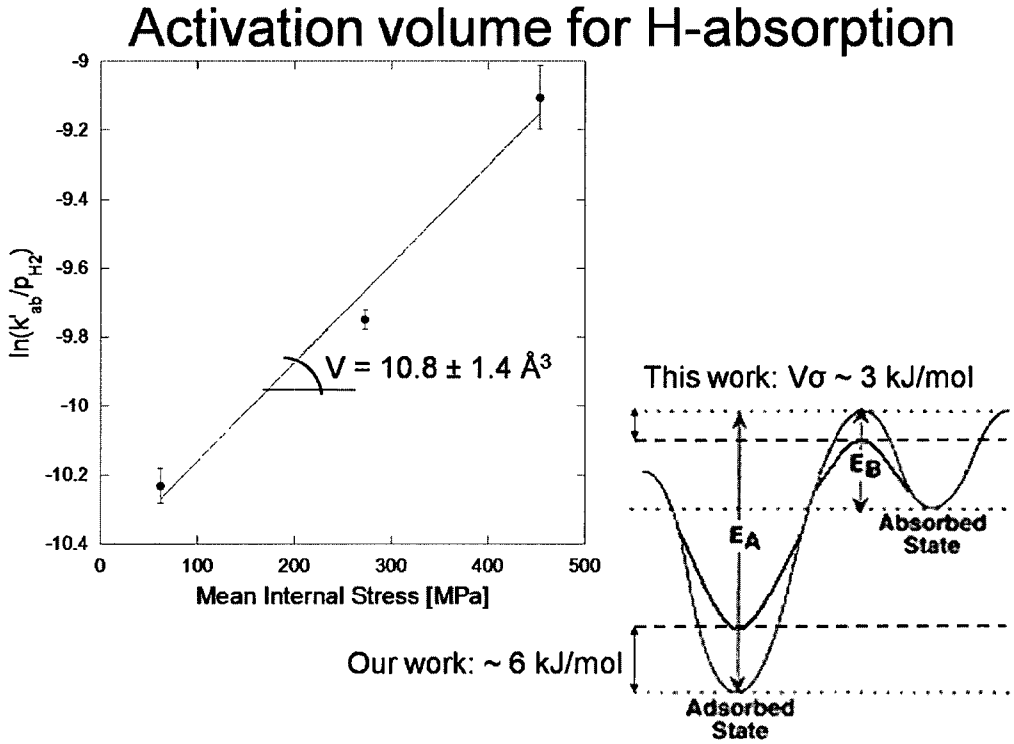

Figure 23

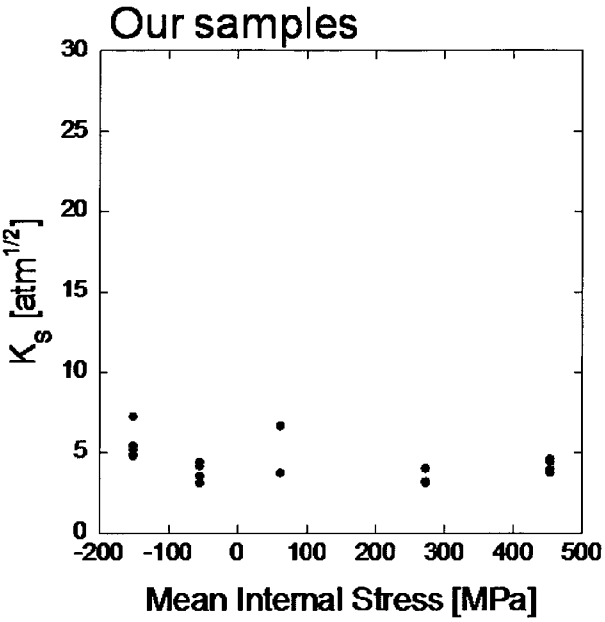

Indicative for a high concentration of defects

Figure 24

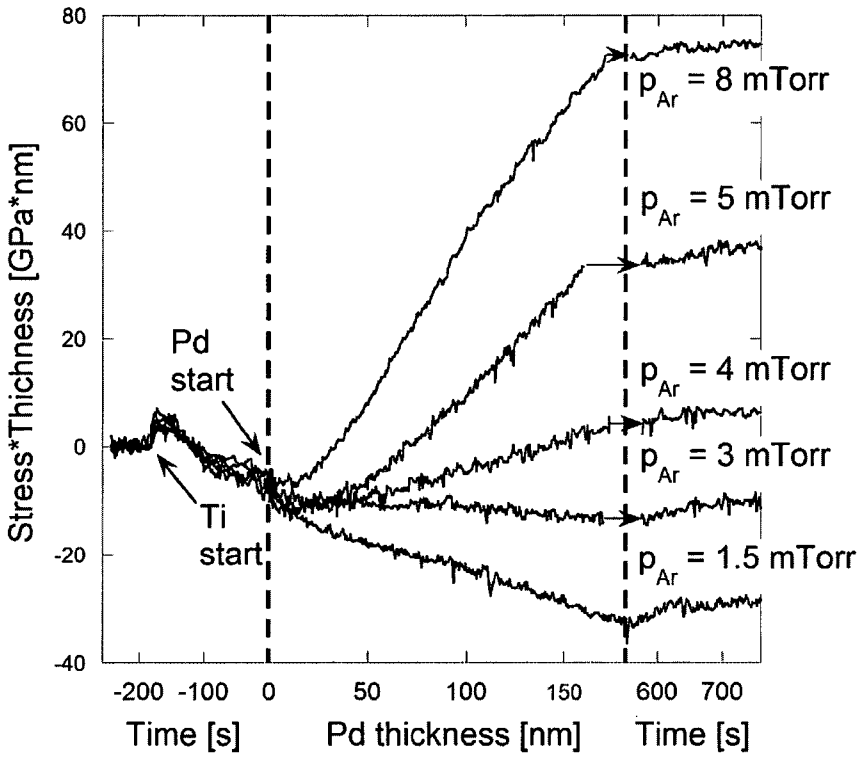

Figure 25

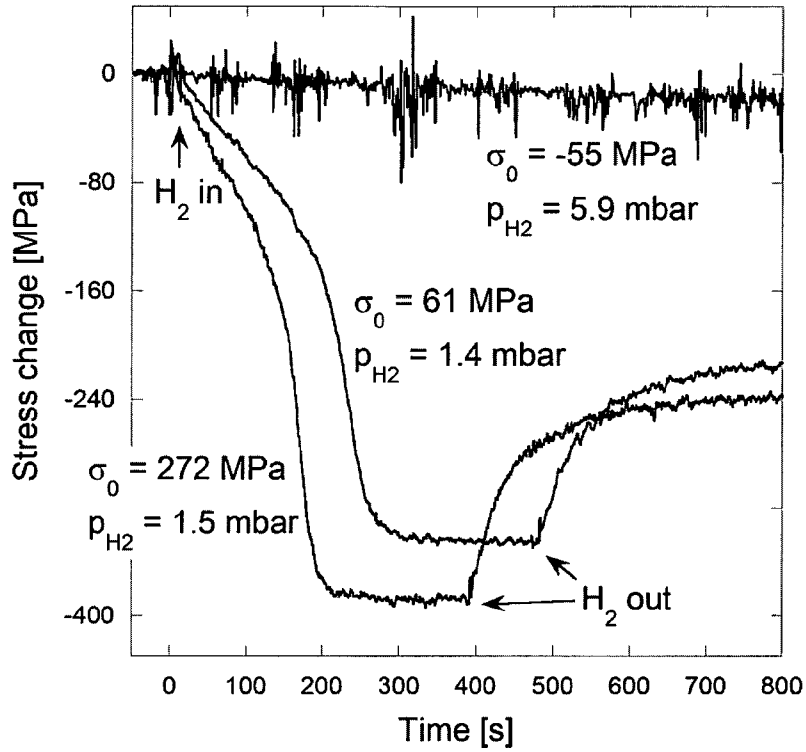

Figure 26

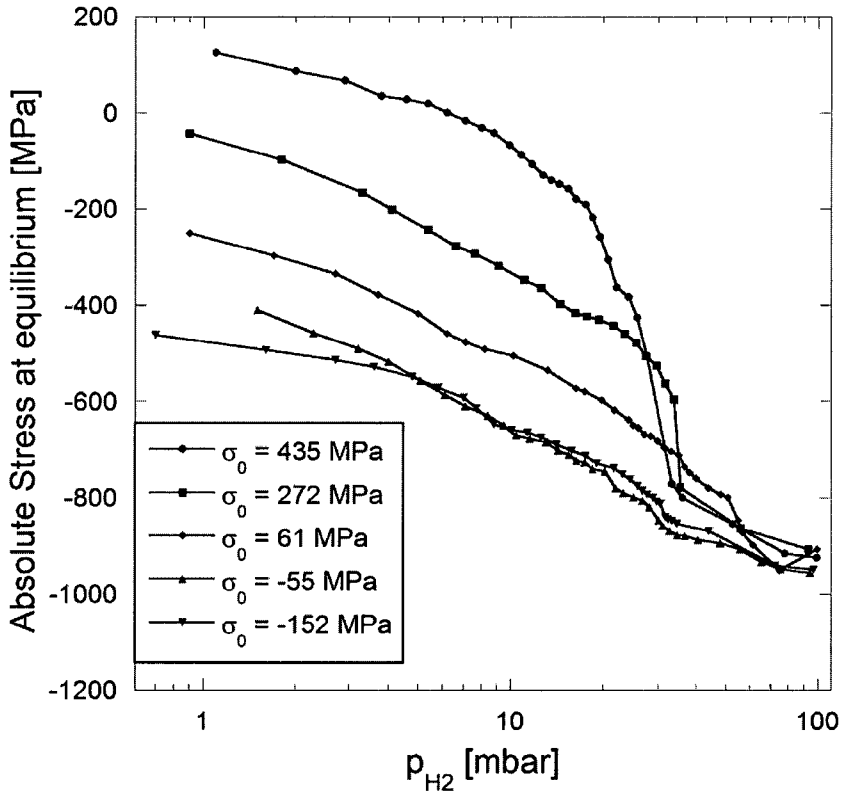

Figure 27

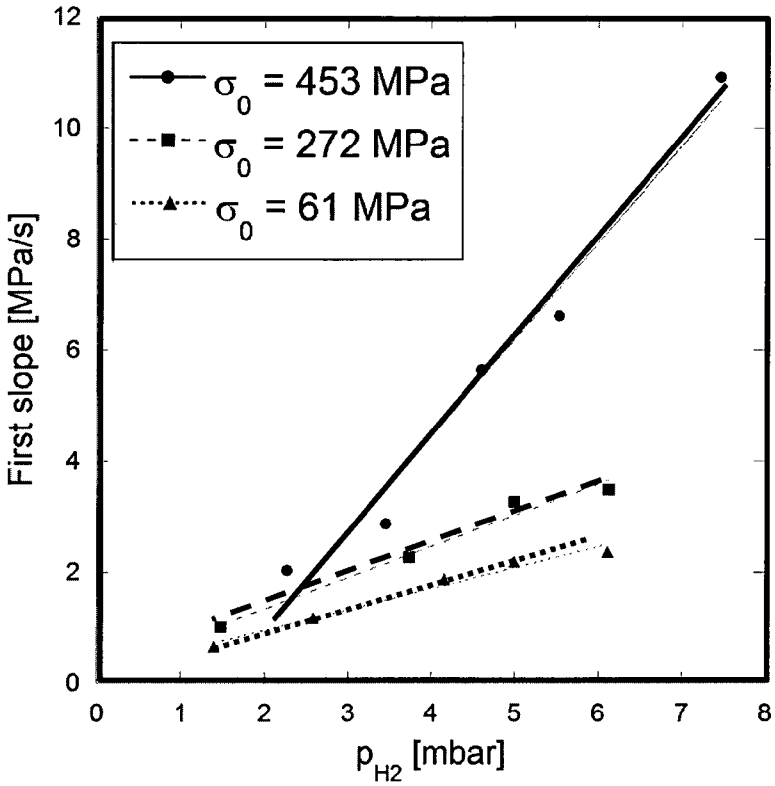

Figure 28

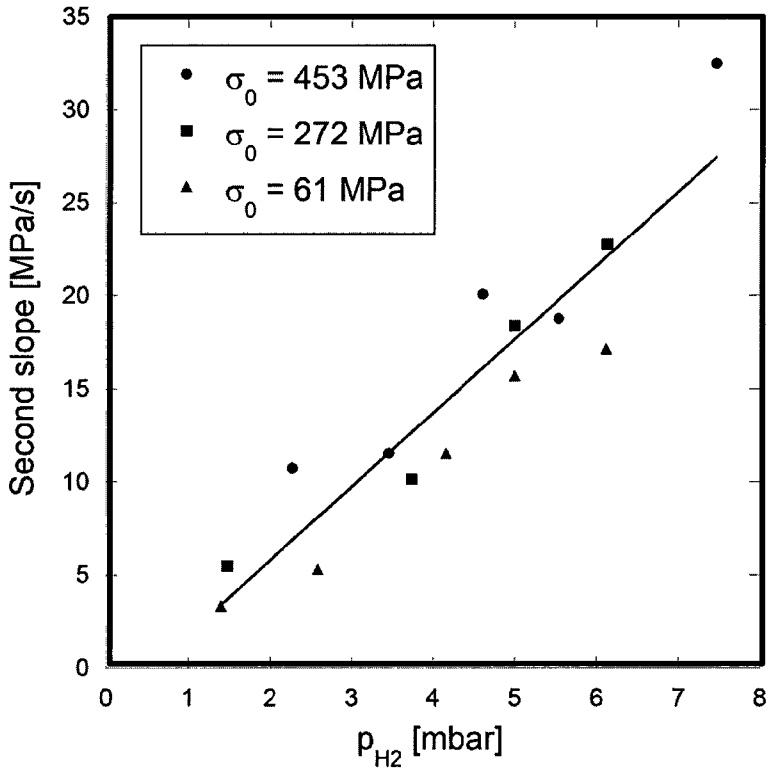

Figure 29

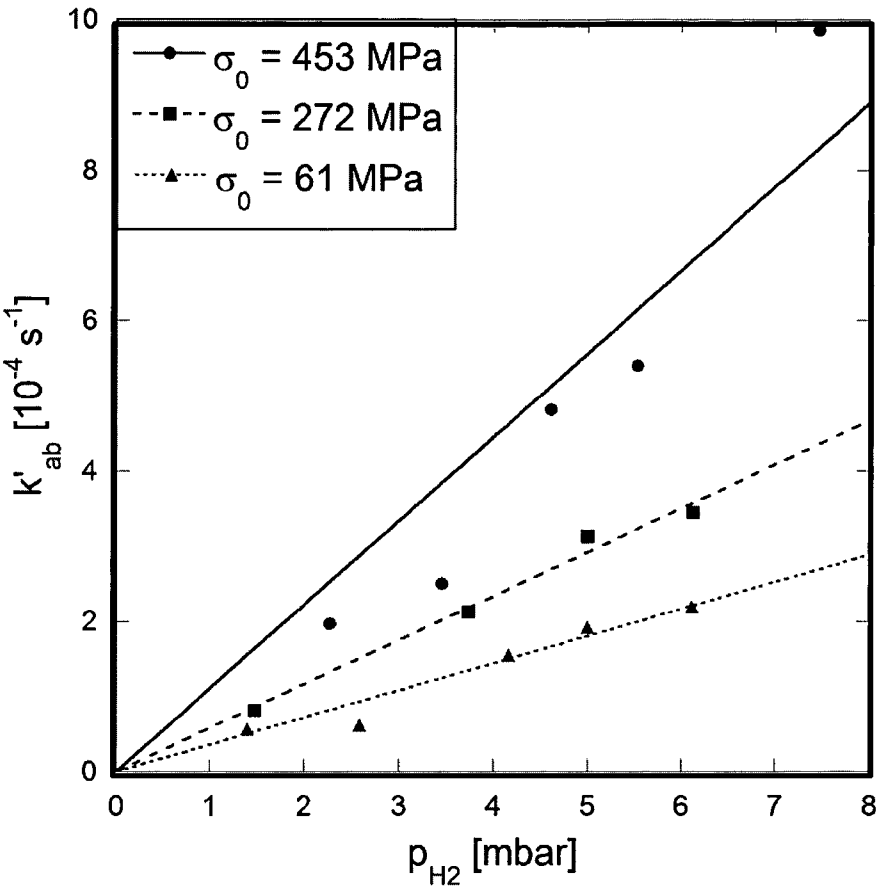

Figure 30

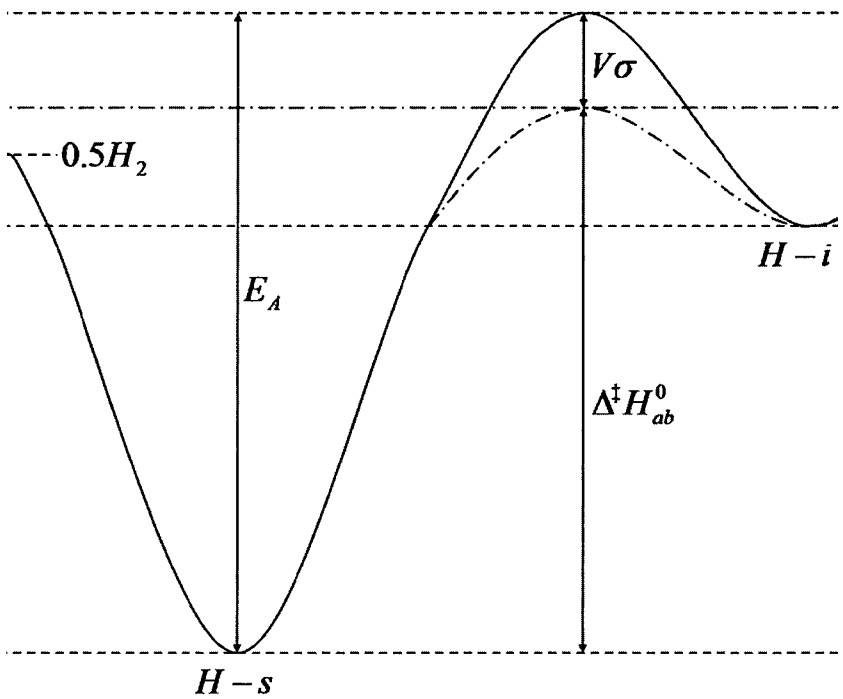

Figure 31

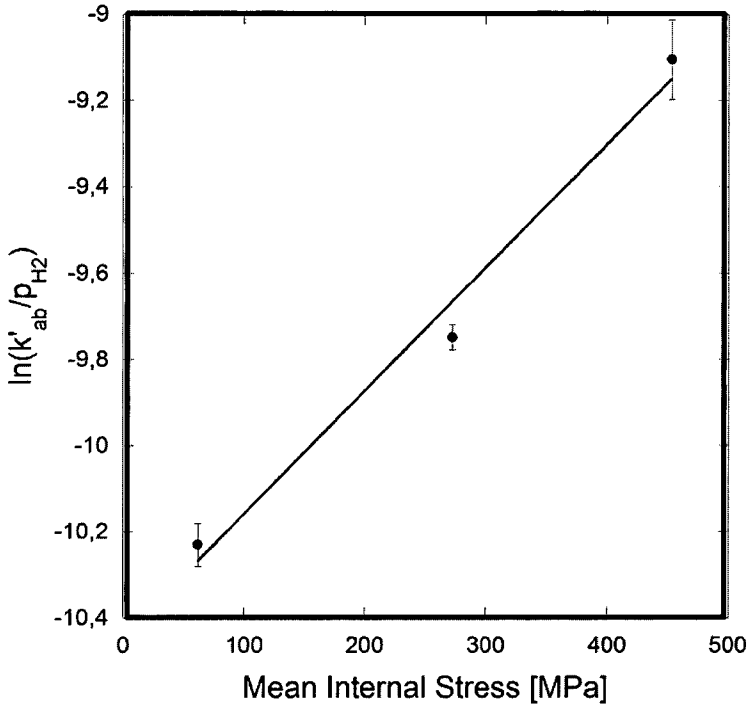

Figure 32

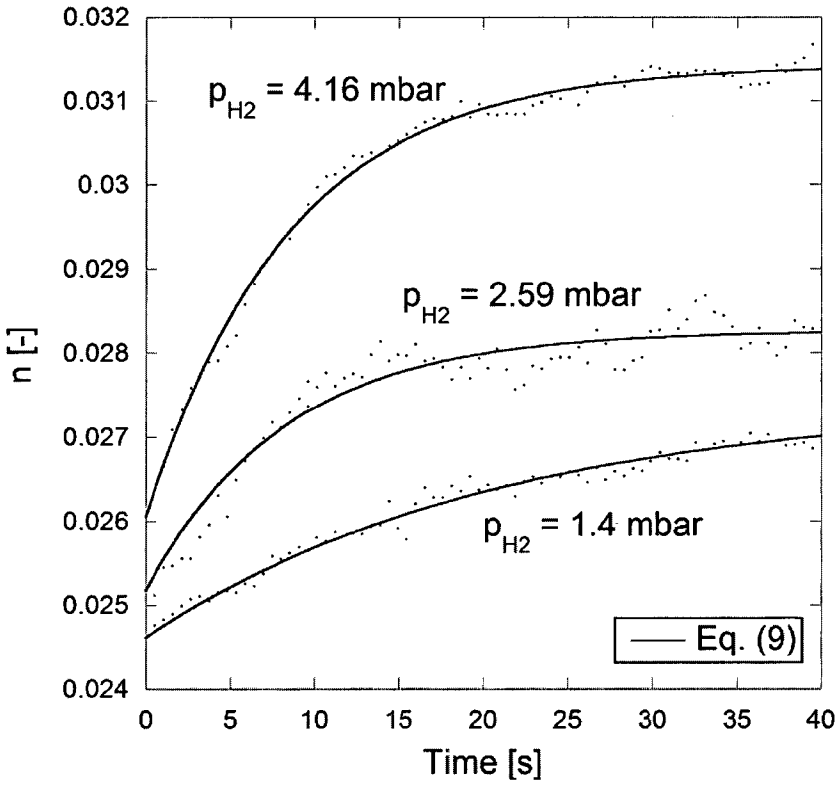

Figure 33

INTERNATIONAL SEARCH REPORT

International application No
PCT/EP2012/058832

A. CLASSIFICATION OF SUBJECT MATTER
INV. C01B3/00 C01B3/02
ADD.

According to International Patent Classification (IPC) or to both national classification and IPC

B. FIELDS SEARCHED

Minimum documentation searched (classification system followed by classification symbols)
C01B

Documentation searched other than minimum documentation to the extent that such documents are included in the fields searched

Electronic data base consulted during the international search (name of data base and, where practicable, search terms used)
EPO-Internal

C. DOCUMENTS CONSIDERED TO BE RELEVANT

Category*	Citation of document, with indication, where appropriate, of the relevant passages	Relevant to claim No.
X	US 2003/026757 A1 (PECHARSKY VITALIJ K [US] ET AL) 6 February 2003 (2003-02-06)	1-6,9,10
Y	abstract figure 1 paragraphs [0025] - [0027]	7,8
Y	WAGNER STEFAN ET AL: "Mechanical stress impact on thin Pd1â xFex film thermodynamic properties", APPLIED PHYSICS LETTERS, AIP, AMERICAN INSTITUTE OF PHYSICS, MELVILLE, NY, US, vol. 92, no. 5, 8 February 2008 (2008-02-08), pages 51914-51914, XP012108068, ISSN: 0003-6951, DOI: 10.1063/1.2841636 cited in the application the whole document	7,8

-/--

[X] Further documents are listed in the continuation of Box C.

[X] See patent family annex.

* Special categories of cited documents :

"A" document defining the general state of the art which is not considered to be of particular relevance

"E" earlier application or patent but published on or after the international filing date

"L" document which may throw doubts on priority claim(s) or which is cited to establish the publication date of another citation or other special reason (as specified)

"O" document referring to an oral disclosure, use, exhibition or other means

"P" document published prior to the international filing date but later than the priority date claimed

"T" later document published after the international filing date or priority date and not in conflict with the application but cited to understand the principle or theory underlying the invention

"X" document of particular relevance; the claimed invention cannot be considered novel or cannot be considered to involve an inventive step when the document is taken alone

"Y" document of particular relevance; the claimed invention cannot be considered to involve an inventive step when the document is combined with one or more other such documents, such combination being obvious to a person skilled in the art

"&" document member of the same patent family

Date of the actual completion of the international search	Date of mailing of the international search report
29 August 2012	06/09/2012

Name and mailing address of the ISA/	Authorized officer
European Patent Office, P.B. 5818 Patentlaan 2 NL - 2280 HV Rijswijk Tel. (+31-70) 340-2040, Fax: (+31-70) 340-3016	Alvarez Rodriguez, C

INTERNATIONAL SEARCH REPORT

International application No
PCT/EP2012/058832

C(Continuation). DOCUMENTS CONSIDERED TO BE RELEVANT

Category*	Citation of document, with indication, where appropriate, of the relevant passages	Relevant to claim No.
A	DELMELLE R ET AL: "In-situ monitoring of hydride formation in Pd thin film systems", INTERNATIONAL JOURNAL OF HYDROGEN ENERGY, ELSEVIER SCIENCE PUBLISHERS B.V., BARKING, GB, vol. 35, no. 18, 1 September 2010 (2010-09-01), pages 9888-9892, XP027235650, ISSN: 0360-3199 [retrieved on 2010-08-25] cited in the application abstract -----	1-10
A	US 2007/025908 A1 (SANDROCK GARY [US] ET AL) 1 February 2007 (2007-02-01) abstract paragraphs [0029], [0141] - [0147] -----	1-10

INTERNATIONAL SEARCH REPORT

Information on patent family members

International application No
PCT/EP2012/058832

Patent document cited in search report	Publication date	Patent family member(s)	Publication date
US 2003026757 A1	06-02-2003	NONE	
US 2007025908 A1	01-02-2007	NONE	